Creep and Elevated Temperature Mechanical Properties of 5083 and 6061 Aluminum

Benjamin William Allen

Thesis submitted to the faculty of Virginia Polytechnic Institute and State University in partial fulfillment of the requirements for the degree of

Master of Science
In
Engineering Mechanics

Scott W. Case
Brian Y. Lattimer
John J. Lesko

December 11, 2012
Blacksburg, VA

Keywords: Aluminum, Mechanical Properties, High Temperature, Creep, Induction Heating

Creep and Elevated Temperature Mechanical Properties of 5083 and 6061 Aluminum

Benjamin William Allen

ABSTRACT

With the increasing use of aluminum in naval vessels and the ever-present danger of fires, it is important to have a good understanding of the behavior of aluminum at elevated temperatures. The aluminums 5083-H116 and 6061-T651 were examined under a variety of loading conditions and temperatures. Tensile testing was completed on both materials to measure strength properties of elastic modulus, yield strength, and ultimate strength as well as reduction of area from room temperature to 500°C taking measurements every 50°C. These tests showed how much the material weakened as temperature increases. Low temperatures had a minimal effect on strength while exposure to temperatures between 200 and 300°C had the most significant impact. Creep testing was also completed for these materials. These tests were completed at temperatures between 200 and 400°C in 50°C increments. Stresses for these tests were in the range of 13 to 160MPa for 5083 aluminum and between 13 to 220MPa for 6061 aluminum. These tests showed a significant relationship between stress and temperature and how changes to one can cause a very different resulting behavior. In addition to the creep testing, three creep models were examined as a means of predicting creep behavior. These models included a power law, exponential, and hyperbolic-sine versions and were able to predict creep results with decent accuracy depending on the stress used in the model.

Dedication

This work is dedicated to my family who has always supported me through all my academic and personal goals. I want to thank them for always being there to talk and give me advice even if they didn't understand what I was talking about. I also appreciate all the help from my uncles, Tom and Mark, who have given me lots of advice and guidance throughout the years.

Acknowledgements

I would like to acknowledge and thank the following persons who made the completion of this work possible.

Dr. Scott Case – Thank you for being my advisor and friend. I want to thank you for your encouragement and guidance through starting as an ESM minor to working my way through graduate school. You helped me find something that I really enjoyed doing and helped me to learn and grow as a student and researcher. I appreciate all your help and patience with me throughout this whole process.

Dr. Brian Lattimer – Thank you for being my advisor and helping me through this entire process. I remember taking your thermodynamics class way back and as sophomore and hearing about your research and thinking it would be very cool to work with you on a project like that. I got the opportunity and have greatly enjoyed the experience.

Dr. Jack Lesko – Thank you for being on my committee. Although we did not get many opportunities to talk, I enjoyed the times we did and the insights you had. I also appreciated all the work you did in the composites class I took. It really helped me enjoy mechanics more and confirmed my choice of mechanics for my graduate studies.

Patrick Summers – Thank you for being and good friend and helping me as much as you did with my research. I appreciate all the hard work you have done helping me get things going and your ability to think of all the little things to try that made testing easier or helped me focus and solve the real issues that were occurring.

Christian Rippe and Yanyun Chen – Thank you for your friendship and help throughout this project. I appreciate the advice and times we were able to put work aside and chat.

Jess Dibelka and Tim Hartman – Thank you for all your help with labview coding and learning all the equipment. It was great getting to know you and you made the lab a much more enjoyable place.

Table of Contents

List of Figures

List of Tables

CHAPTER 1 – Introduction

1.1 Background

Aluminum has been considered a source for naval ship construction dating back to 1895. Its first uses were very limited in scope; only being used as topside fittings for the torpedo boats intended for use with the USS *Maine* battleship **[1]**. However, initial attempts turned out poor results as the aluminum used exhibited corrosion. The first aluminum deckhouse for the U.S. Navy was implemented in 1889 for use on the torpedo boats *Dahlgren* and *Craven*. Unfortunately, these fared just as poorly as the previous attempts and aluminum was abandoned as a structural material for almost 40 years.

It was not until 1935 that aluminum was reintroduced as a material for deckhouses. It was used with a combination of mild steel to provide a lighter weight and lower cost alternative to using steel alone. This reestablishment of aluminum was spurred by the discovery that introducing magnesium silicate into the aluminum would provide a good corrosion resistance and strength. The alloy was known as 6061, but was limited in its use to riveted construction due to loss of strength when welded. Having a specialized use with only riveted construction, an alloy had to be developed that could be used with welding. The solution was a weldable, corrosion-resistant, 5000 series aluminum.

Three main properties of aluminum have been considered throughout history as relevant concerns with aluminum construction on naval ships. Corrosion resistance, weldability and fire resistance have been some of the major factors considered when determining materials and usage. Fire resistance has always been a concern, but many people thought it would not be a huge issue because steel frames and reinforcement would hold the structure until repairs could be done. This belief was proven to be incorrect after two fire related incidents occurred. One of the first substantial fires on a naval ship occurred in 1975 aboard a guided missile cruiser. A large fuel spill caused a fire that completely burned the aluminum deckhouse on the ship. Another well-known incident happened in the Falklands in which the British Navy frigate HMS *Sheffield* fared no better against a fire with its steel deckhouse **[1]**. This showed that fire is a very serious concern around aluminum, and it is very important to have a sound understanding of the materials under high temperature situations.

What is evident from the history of aluminum in the Navy is that its uses have been very limited to deckhouses and superstructures. The recent history of aluminum has seen its growth with usage in hulls and main structural components of ships such as the Littoral Combat Ships (LCS) and the Joint High Speed Vessel (JHSV). This makes the characterization of aluminum all the more important. If a fire on a ship with an aluminum deckhouse was an issue, one could only imagine what would happen to a ship with an entire aluminum hull.

1.2 Literature Review

As just discussed, aluminum has been used in many applications for a long period of time. Therefore, research has already been conducted on the material in a variety of fashions. While these particular materials and tempers may not have specifically been examined, similar materials have been providing a basis on which to compare this work with.

When examining a new material it is very important to have an understanding of the materials strength characteristics. Work by Voorhees and Freeman, as part of an ASTM report of elevated temperature properties of aluminum, is major effort to characterize strengths of most aluminums and a variety of temperatures **[2]**. Their work determined some strength properties of similar materials, but different tempers, used in this work, and established a good base for comparison.

While Voorhees and Freeman reported values from high temperature testing, they did little to explain their methods for heating. Völkl and Fischer described using an ohmic heating system to perform ultra-high temperature, up to 3000°C, mechanical tests on oxide dispersion hardened alloys, super alloys, and metallic iridium **[3]**. While they had success with this method up to temperatures well beyond the range examined in this work, ohmic heating was not available. However, induction heating was, and Codrington et al. showed how an induction heating system could be utilized for mechanical testing of steels and aluminums **[4]**. Their work captured the abilities of an induction heating system and its ease of use with standard lab equipment, i.e. extensometers.

Other tensile characterization of aluminums focused on looking at strength behavior as a function of strain rate. Taleff et al. examined aluminum-magnesium alloys under elevated temperatures, up to 500°C, over 5 orders of magnitude of strain rates. Conclusions from their work showed how the presence of magnesium grains in the aluminum could account for high elongations seen in 5083 aluminum **[5]**. Following this train of thought, works by Harun and McCormick and Huskins et al. have examined how precipitation hardening and different grain sizes, respectively, affect the mechanical response of aluminum-magnesium materials **[6, 7]**. It was determined that grain size was not so much a driving force as the type and behavior of the dislocations caused by grain movement. Also work by Van Liempt and Sietsma investigated how strain-rate plays an effect on work hardening, a phenomena present in 5083 aluminum. Their work goes on to explain how the presence of negative strain-rate sensitivity causes plastic deformation to become unstable **[8]**.

As mentioned earlier, similar materials to the ones tested in this work have been examined and strengths characterized at elevated temperatures. More testing by Taleff et al. looked at several 5000 and 6000 series aluminums at elevated temperatures. They found that the 5000 series aluminum exhibits a high tensile ductility while the 6000 series is less ductile, but stronger **[9]**. Ozturk et al. examined a 5052 aluminum measuring tensile properties up to temperatures of 300°C. Results from this work showed behavior very similar to 5083 where high elongation occurs around 300°C as well as a large

decline in strength **[10]**. For the 6000 series, Khalifa and Mohmoud examined a 6063 alloy and how mechanical properties are influenced by slight changes to the composition **[11]**. One of the more relevant examples of other aluminum testing is work done by Amdahl et al. where different 5000 series aluminums were examined as part of a naval ship structure **[12]**.

More relevant examples with respect to materials tested include work by Das et al., Clausen et al., and Leitão et al. In Das' work, high temperature deformation was examined for 5083 finding a transition from ductile to brittle failure behavior around 420°C **[13]**. Clausen examined the flow and fracture behavior of 5083 examining how sample geometry plays a role in the strain hardening behavior and its disappearance with increasing temperature **[14]**. Finally Leitão's work was completed on 5083 and 6082 aluminum. However, more emphasis was placed on welds – a topic that is not covered in this work – but the base materials were characterized showing the stress-strain behavior at elevated temperatures for both materials **[15]**.

The quasi-static mechanical property characterization is very important to know and understand what affects its behavior, but it is not the only aspect of this work. Creep behavior is also examined and modeled.

Kaibyshev et al. examined a modified 5083 aluminum alloy looking at the effects of temperature and stress on strain rate and the presence of a threshold stress **[16]**. This work found that stress applied at a temperature has a substantial impact on the resulting strain rate. Behavior varies whether it is a low stress (less than 3MPa), intermediate stress (between 3 and 100MPa), or a high stress (greater than 100MPa). Other work was done by Yavari et al. looking at an aluminum-5% magnesium alloy and Park examining a 6061 alloy **[17, 18]**. Both of these works looked to examine creep testing over a range of temperatures and determine properties of activation energy and creep model parameters. Harper and Dorn did an examination on high purity aluminum focusing mainly on creep near its melting temperature **[19]**. The main focus was to examine and model the viscous behavior of the aluminum at these temperatures.

Creep modeling is the final aspect of this work. This portion is very useful as it allows for prediction of creep behavior without performing long creep tests. Before looking at the creep model, Feltham and Meakin looked at the activation energy and showed that it can only be determined by looking at strain rates from the same stress, but different temperatures **[20]**.

Some of the first major advances in modeling came from the work of Dorn **[21]**. He worked on developing creep models to predict high and low stress creep curves with the use of two equations. Later on, a model proposed by Garofalo successfully measured high and low stress creep curves using a single equation **[22]**. The main focus of their work was to model secondary creep. Others have worked on expanding this in to the tertiary and primary creep regions. Harmathy worked on expanding Dorn's creep model to include primary creep, while Maljaars examined modeling an entire creep curve that includes the tertiary region **[23, 24]**. Even though these models are widely used and

accepted, a book by Penny and Marriott collects them and breaks them down and describes their different components **[25]**.

1.3 Research Objectives

The focus of this research is to characterize the behavior of 5083-H116 and 6061-T651 aluminum under various loading and high temperatures. Elevated temperature mechanical testing is used to determine strength properties of elastic modulus, yield strength, and ultimate strength. Creep testing is performed to determine the material behavior with a load during a fire scenario.

The materials used for this work are common aluminum alloys used in shipbuilding. While a 6082 alloy would be more representative of a ship material, it is commonly used overseas and not readily available in the United States; therefore, the 6061-T651 was chosen as a substantially equivalent alloy in strength and material behavior. 5083-H116 and 6061-T651 will be referred to as 5083 and 6061 respectively for simplicity throughout this work.

Elevated temperature mechanical testing will be used to characterize the strength of the material at temperatures that range from room temperature to near the melting temperature, around 500°C. Strength properties determined from testing are elastic modulus, yield strength, and ultimate strength. The goal from this testing is to have a complete understanding of the strength of the material as a function of increasing temperatures.

Creep testing will also be performed as a part of this work. Testing will be done with various combinations of temperature and loads. The important data from these tests is the steady-state strain rate that will be used for developing a model to predict behavior of the material under any kind of load and temperature combination. A model like this will be useful for finite element modeling of the materials in a structure with elevated temperatures.

CHAPTER 2 – Experimental Methods

2.1 Introduction

A series of elevated temperature tests were performed on 5083 and 6061 aluminum samples. Tests were performed using two methods. The first was a mechanical test in which the sample was under a constant strain rate, and the second was a creep test where a constant load was applied. An MTS load frame was used to perform the tests and an induction heater was used to control the temperature. Other instruments such as extensometers, infrared thermometers, and data acquisition equipment were used as means of gathering and recording the necessary data.

2.2 MTS Load Frame

A Material Tests System (MTS) model 880 load frame was used for tensile and creep testing. The MTS load frame provided all the necessary functions to easily perform high temperature testing. Easy access to the front and back of the machine gave space for induction heating and extensometer equipment. Also the controller for the machine had the ability to switch between load and stroke control to perform tensile and creep testing without any modifications. Shown in Figure 2-1 is the MTS load frame and controller.

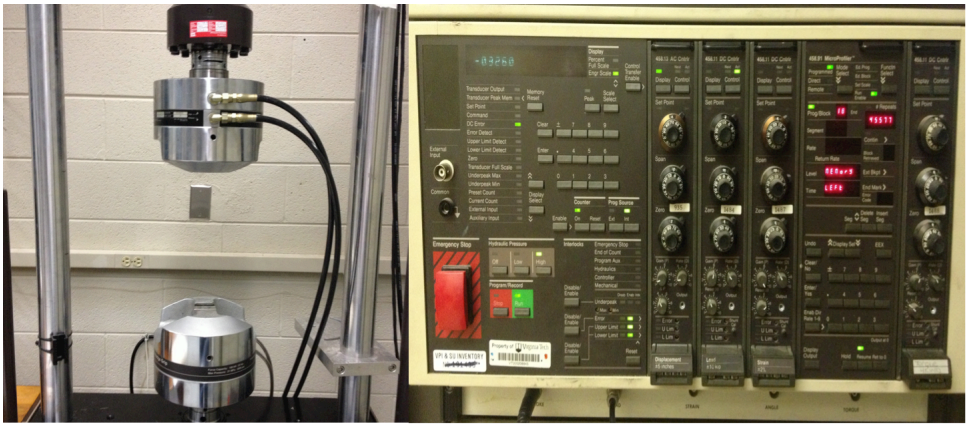

(a) **(b)**

Figure 2-1: MTS load frame and controller

The load frame, Figure 2-1a, has a stationary upper crosshead and a moving lower actuator arm. Hydraulic grips with water-cooling are another feature of the load frame. The grips are not rated to withstand high temperature so water-cooling is a necessity to prevent damage to the actuator from overheating. The cooling also provides a known, consistent thermal boundary condition for all testing.

Running the load frame is entirely operated from the controller, Figure 2-1b. There are many features on the controller, but three are important for this work. The 458.13 AC and 458.11 DC controllers are used for stroke and load control respectively, and 458.91 MicroProfiler is used for running test programs. The stroke controller is

equipped with a ±5in displacement card and the load controller has a ±10kip load card. Another feature that makes this controller ideal for high temperature testing is the ease of switching between the load and stroke controller. This makes it simple to heat a sample in load control then switch and run a test in stroke control. There are also BNC outputs for load and stroke that are used with the data acquisition equipment. The MicroProfiler card is a programmable card that is used to run the tensile and creep tests. A ramp rate and desired load or stroke level can be set and executed for different testing scenarios.

2.3 Heating Method

High temperature characterization of the material is the main focus of this work; therefore, the method of heating the material is a very important consideration. While heating aluminum seems like it should be a straightforward task, there are multiple ways to approach it. Three methods for heating were considered: a single-zone split tube furnace, three-zone split tube furnace, and induction heating.

2.3.1 Comparison of Heating Methods

As mentioned, three methods of heating were researched to determine the best way to effectively heat the materials for testing. Three criteria were considered when selecting the best heating method: heating capabilities (i.e. temperature gradient and heating rate), compatibility with available equipment, and cost.

The first method, the single-zone split tube furnace, is an electrically powered furnace that encloses the sample in a cylindrical shell. There are heating coils embedded in the insulation that are heated based on a feedback control that is controlled by a thermocouple near the heating elements. An example of a single-zone split tube furnace is shown in Figure 2-2.

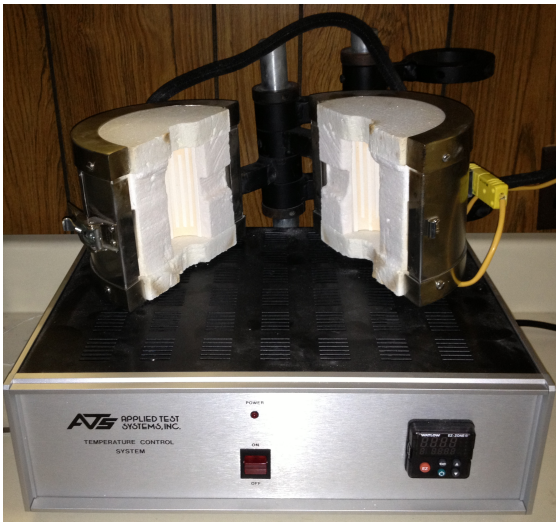

Figure 2-2: Single-zone split tube furnace and controller

Advantages of this method are its compatibility with available equipment and cost. The arms coming off the back of the furnace are designed for use with the available load frame and the slot down the front allows access for an extensometer. Also for a relatively low cost, the furnace is able to heat the aluminum. However, the temperature gradient, Figure 2-3, is very significant and not desired for testing.

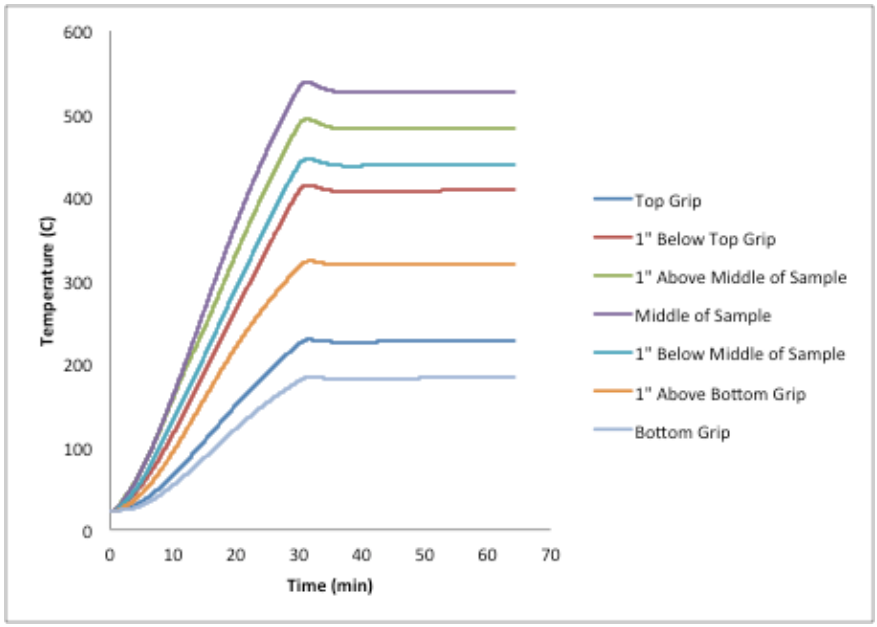

Figure 2-3: Temperature gradient from single-zone split tube furnace

To measure the temperature, thermocouples were placed 1in apart down the length of the sample. Therefore, the lines in Figure 2-3 each represent a thermocouple measurement on the sample. To mount the thermocouples, a hole was drilled through the sample and an aluminum nut and bolt kept the thermocouple in contact with the sample throughout the heating process. The extensometer that will be used for testing has a gage section of 2in that would correspond to the range 1in above and below the middle point. In this region alone, the maximum temperature of the furnace temperature varies by 80°C. The limitations of the furnace do not allow for good control over the heating rate.

The second method is the three-zone split tube furnace. This method is very similar to the single-zone in the manner that it uses heating elements to radiate the sample and heat it to the desired temperature. The difference is what its name indicates, it has three-zones. Three separate sections of heating elements allow for better control of temperature by controlling each zone with a separate controller.

Figure 2-4: Three-zone split tube furnace [26]

An example of a three-zone furnace is shown in Figure 2-4. However, this manner of heating was not pursued. While the temperature gradient would be significantly better, it was not easily compatible with the rest of the equipment; therefore, rendering it not a feasible option.

Finally, the induction heater was last method examined for heating. An induction heater works by running an electric current through the copper coils around the sample. The alternating current passing by the sample causes the molecules in the sample to excite and heat up. An example of an induction heater is shown in Figure 2-5.

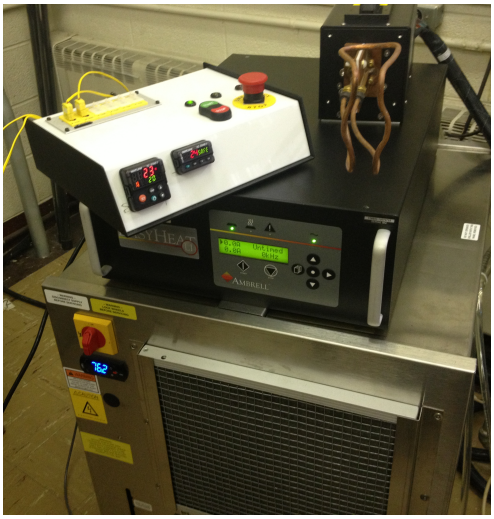

Figure 2-5: Induction heating system

Considering the criteria for heating, this is clearly the most expensive option, but is very compatible with current equipment since different coils can be designed for

various situations. As a result of two equally compatible systems, temperature gradient played a major factor in the final decision.

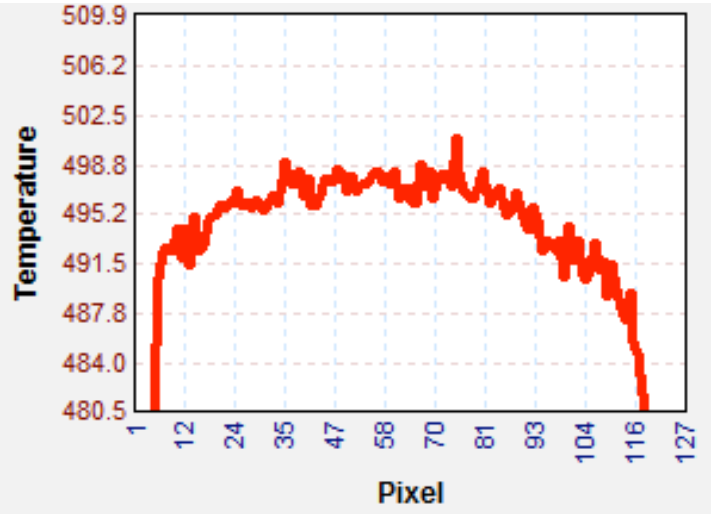

Figure 2-6: Temperature gradient for induction heater

Figure 2-6 shows that even at 500°C, the temperature gradient over the 2in extensometer gage length is approximately 10°C. Also the proportional-integral-derivative (PID) controller allows for excellent control over the heating rate.

In summary, the three-zone furnace was not feasible due to incompatibility with current equipment; the single-zone furnace, while financially the best option, caused unacceptable temperature gradients along the sample, and the induction heater provided the most even heating and heating rate control, but is very expensive. Ultimately, the benefits of the induction heater outweighed the cost, making it the best option and clear choice for heating for this work.

2.3.2 Induction Heating and Coil Design

Since induction heaters heat the material by running an electrical current through coils, the design of the coils is very important to ensure even heating of the sample. Coils can be designed in almost every imaginable way to provide heating for any kind of situation. The standard design is typically a circular pattern that has an opening in the middle for the sample to pass through. While this is the most efficient method, it is not always ideal for testing. This design limits use of additional equipment because the coils block the sample so one cannot tell what is happening in the heated zone. For this work, two coil designs were used. Figure 2-7 shows what the two designs look like on a sample.

(a) **(b)**

Figure 2-7: Coil designs for induction heater

Figure 2-7a shows the first design that was used for all 6061 testing. In this design the circular coils at the top and bottom provide efficient heating that will start at those points and spread to the center. The points in the middle provide a little extra heat to that spot to make it the hottest point on the sample. Making it the hottest point helps to guarantee that necking and failure will always occur in the same location. Adjustments can be made to the coils to get better gradients at different temperatures by changing the spacing between the top and bottom circular coils and/or changing the distance between the middle coils. However, there is a drawback to this design. When high elongation is present, such as seen with higher temperature tests, the necked region starts to move within the circular region where heat is generated. Temperature increases up to 50°C can occur as a result. The solution to this was a different coil design, Figure 2-7b.

In this design, the coil is brought straight down the side of the sample. The middle of the coil was also bowed out to lower the peak temperature that occurs in the center. Unlike the previous design, this coil starts heating in the center and spreads to the ends. This coil also helps address the issue with necking since it is center heating instead of end heating.

2.3.3 Induction Heater

Effort has been made to set up the induction heating system in a way that allows for efficient heating and compatibility with other equipment. The induction heating system, Figure 2-4, has multiple components that work together to provide the most effective test setup possible. Parts of the system include the chiller, which helps with keeping the system from overheating and cooling the coils immediately following a test. The actual induction heater has the ability to run a test, but for simplicity, control is provided by a Watlow PID controller. A temperature is set on the PID controller and ramps at a specified rate to the temperature that is determined by an infrared thermometer looking at the sample. The last piece of the system is the work head to which the coil is attached and used for the actual heating.

2.4 Additional Instrumentation

The MTS load frame and induction heater are two essential pieces of equipment for testing, but they are not the only items needed to effectively complete this work. Other equipment such as extensometers and signal conditioners for strain measurement, infrared thermometers and cameras for temperature measurement, and a data acquisition system to record and process the data were used to accomplish these tasks.

2.4.1 Extensometer

The classic instrument for measuring strain is an extensometer. It is a very simple and effective tool for measuring strain during a mechanical or creep test. The extensometer utilized for this testing in this work consisted of a high temperature mechanical and laser extensometer.

2.4.1.1 High Temperature Extensometer

An Epsilon Model 3448 High Temperature Furnace Extensometer was selected. This extensometer has a 2in gage length and can travel 1in in tension and -0.4in in compression corresponding to +50% and -10% strain respectively. Other characteristics of this extensometer model include a 10V excitation and full Wheatstone bridge configuration. This extensometer is shown in Figure 2-8.

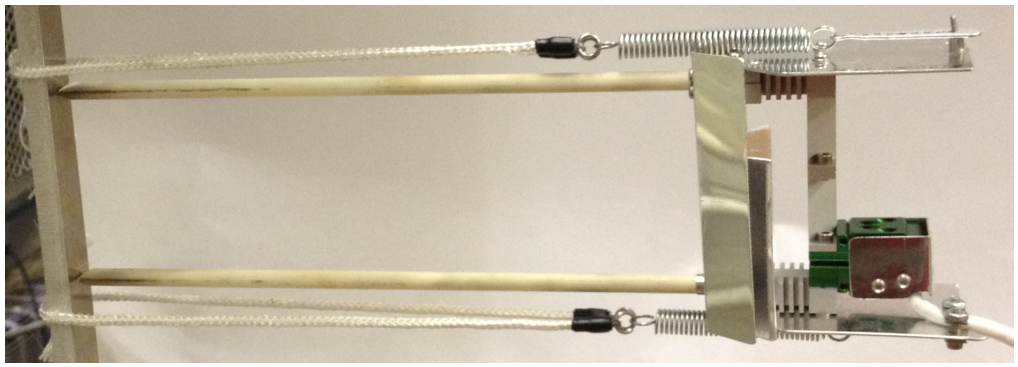

Figure 2-8: Epsilon Model 3448 High Temperature Extensometer

The features of this model include the ceramic rods that allow for use with an induction heater since there are no metallic elements in the rods. There are also fiber cords to hold the extensometer on the sample. Again, there is no metallic component in the cords making them compatible with the induction heater. A Vishay 2310 Signal Conditioning Amplifier is used in conjunction with the extensometer. The amplifier is shown in Figure 2-9.

Figure 2-9: Vishay 2310 Signal Conditioning Amplifier

Features of this signal conditioner include an auto-balance and trimmer for zeroing the signal and fine-tuning the value. Other functions are the ability to set different excitation voltages, and gain adjustment to set the full-scale value for the extensometer. Voltage output from the signal conditioner is measured by the data acquisition system for recording the strain data.

2.4.1.2 Laser Extensometer

While the Epsilon high temperature extensometer is an effective tool, it still has its limitations. The most glaring of the limitations is its 50% maximum strain measurement. While 50% is acceptable for low temperatures with low elongations, it is not able to capture the full stress-strain profile of the high temperature, high elongation tests. As a solution for this dilemma, a laser extensometer from Fiedler Optoelektronik GmbH was employed. Shown in Figure 2-10, the system encompasses the laser and receiver, power supply, and computer system.

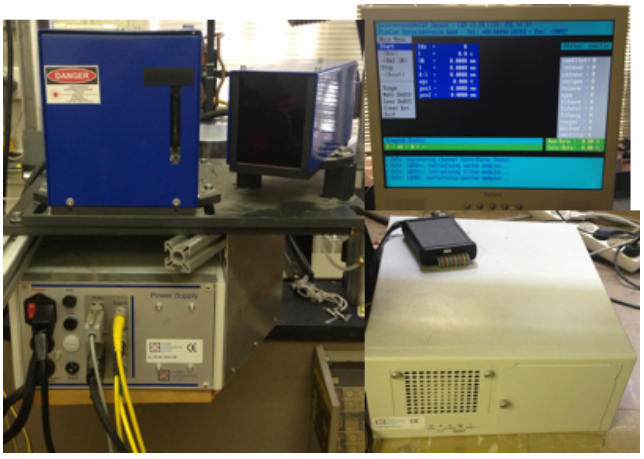

Figure 2-10: Laser extensometer system

Having a full computer system as part of the extensometer setup allows for a more customizable setup. Most importantly, it can be set to measure strain over 50%. This systems works by painting a white strip on a black sample, Figure 2-11, and the system recognizes the edges created by the contrast in color and uses those boundaries as the basis for measuring strain.

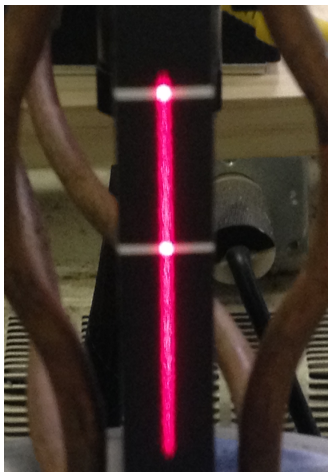

Figure 2-11: Painted sample for use with laser extensometer

Figure 2-11 shows that the laser extensometer can measure strain over a limited range. Positioning the strips becomes an important part of the process. The idea is to have the stripes far enough apart to capture the full elongation and strain of the material, but close enough to not go outside the measurement zone during a test.

Overall, the laser extensometer is a suitable alternative to the mechanical extensometer. It has the ability to measure strain up to any point, but it does require more sample preparation time as well as a trial and error to learn the system and get the desired results.

2.4.2 Temperature Measurements

Temperature was measured using two different devices, an infrared thermometer (pyrometer) and an infrared camera (IR camera). The first device, the pyrometer, provides a point measurement of temperature. Measurements are taken over a very small area and averaged to display the temperature at that certain spot. On the other hand, the IR camera is an actual camera. It has a much larger field of view to look at the temperature profile over the entire sample.

2.4.2.1 Infrared Thermometer

As previously mentioned, the pyrometer measures a small area to give a point measurement of temperature. The particular model used in this work, a Micro-Epsilon thermoMETER CT-SF22, has a measurement area, or spot size, of 7mm at a distance of 100mm. Other features of this model include a temperature measurement range between -50 to 975°C, adjustable emissivity and transmissivity, output signals of type K and J

thermocouple, voltage and amperage, and a system accuracy of ±1°C. Figure 2-12 shows this type of pyrometer.

Figure 2-12: Micro-Epsilon CT-SF22 infrared thermometer

Accompanying the pyrometer is a laser-sighting tool, also from Micro-Epsilon, and a zinc-selenide plano-convex lens from Thorlabs. These tools, in conjunction with the pyrometer, help attain very accurate temperature measurements. The laser-sighting tool is simply a laser that shows the location of the temperature measurement from the pyrometer. They are both on a bracket, Figure 2-13, that can pivot left and right to assure consistent alignment with the center of the sample.

Figure 2-13: Infrared thermometer with laser-sighting tool and focusing lens

The lens then focuses the spot size from the pyrometer from approximately 7mm to approximately 1mm. Determination of the new spot size is shown in Figure 2-14. With a focal length of 6in, basic trigonometry can be used to find the new spot size.

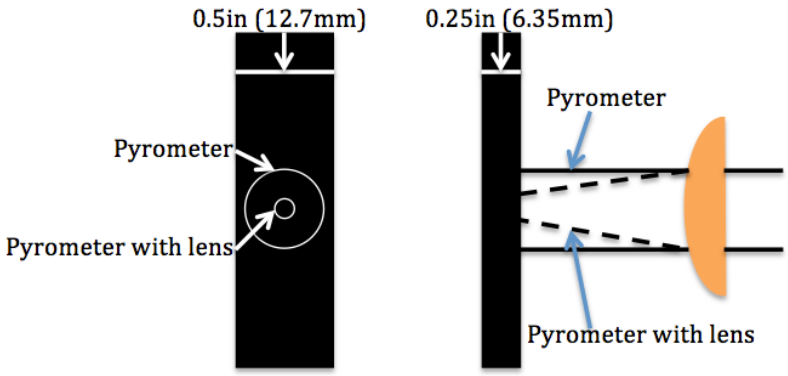

Figure 2-14: Front and side views of spot size of focusing lens

Figure 2-14 shows what would happen if necking occurs around the measurement location without the lens. The pyrometer will start to average the temperature of everything it can see in the room and give a lower temperature than the actual sample. Using the lens helps to prevent this issue and allow for better temperature control for the duration of a test.

2.4.2.2 Infrared Camera

To capture the entire temperature profile of the sample during testing, an infrared (IR) camera by FLIR systems is utilized. With the ability to see the whole sample, temperature gradients can be measured and monitored throughout the duration of a test. A standard setup for an IR camera, Figure 2-15, is to place the camera on a tripod and use computer software, ExaminIR, to view the image.

Figure 2-15: FLIR infrared camera

Capabilities of the IR camera include many adjustable parameters such as emissivity and transmissivity. Temperature can also be measured over the range of -40 to 2000°C with an accuracy of ±2°C. Other functions of the software include options to take pictures of the sample, record a video, and look at point, line, circular, etc. temperature profiles at different locations. A typical screen on the software side looks like Figure 2-16.

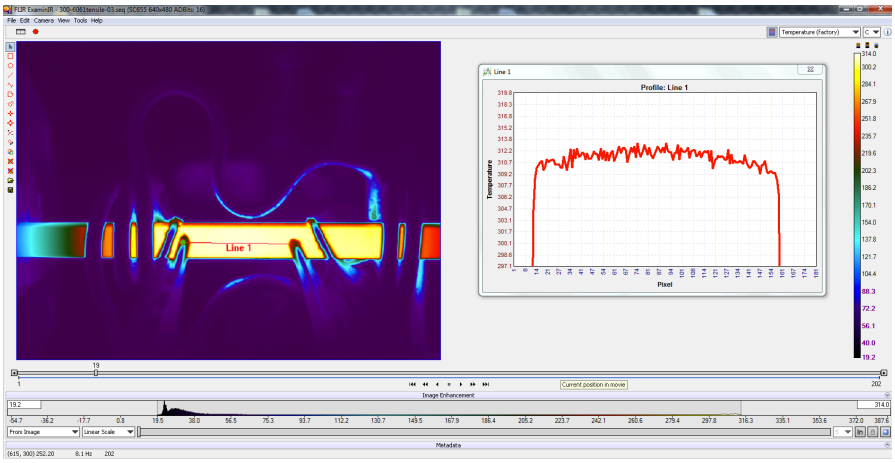

Figure 2-16: ExaminIR software screenshot

A sample is heated to 300°C and a line is drawn across the middle to observe the temperature profile throughout the test. Using this system on all testing provides a means to show whole sample profiles and information that cannot be detected with a thermocouple, pyrometer, or other contact measuring devices.

2.4.3 Data Acquisition System

One of the most important pieces of equipment for testing is the data acquisition system. A common option is a National Instrument (NI) compact data acquisition system (cDAQ). For this work, a cDAQ-9174 model was selected. This model has the chassis with four slots for measurement cards and an USB output to a computer. Measurement cards used with the cDAQ are the NI 9215 voltage card and the NI 9211 temperature card.

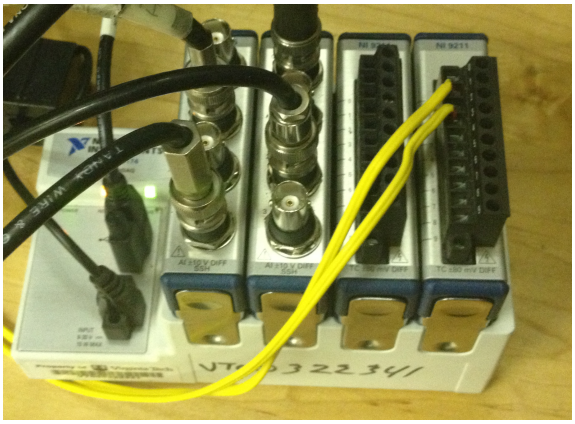

Figure 2-17: Data acquisition system

Shown in Figure 2-17 is the cDAQ system with two of each type of measurement card. The NI 9215 measures voltage from one of four BNC cable inputs. Voltage can be measured between -10 to 10 V, and can be adjusted to other ranges within the ±10V. On the temperature side, the NI 9211 cards receive bare wire inputs. Measurements can be

made using any thermocouple type, J, K, N, etc. and can measure in any temperature unit, °C, °F, K, or R.

While the measurement cards acquire the data from the other systems, they do not perform the processing and recording. That is accomplished on the computer using the National Instruments software, LabView. Built specifically to work with NI data acquisition equipment, LabView is used to read the data from the measurement cards and process and saving the results. Two windows are present in the software, the front panel where graphs and numbers are displayed, and the block diagram where the code is written.

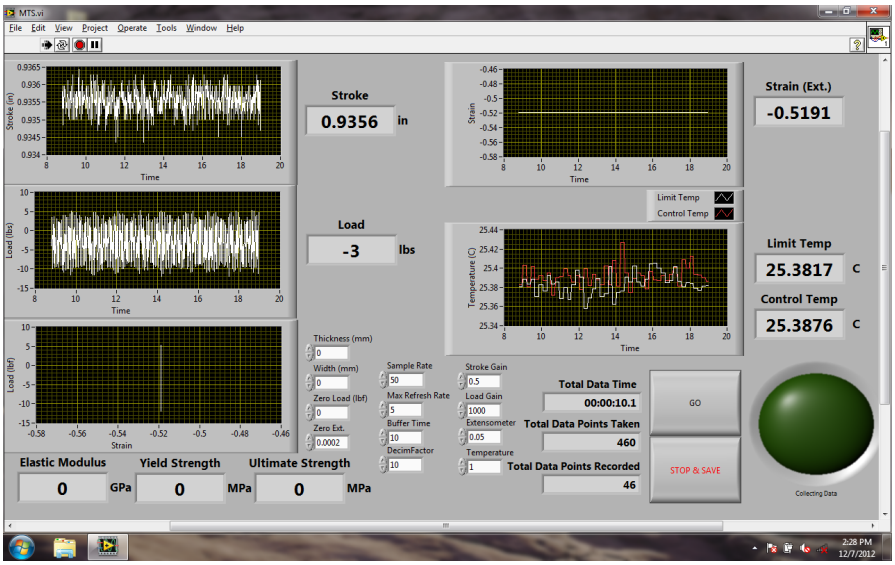

Figure 2-18: Labview front panel and block diagram

The front panel, Figure 2-18, has plots for displaying load, stroke, strain, temperature, and load-strain curves. It will also display the numeric values as they are measured and calculate elastic modulus, yield strength, and ultimate strength upon completion of a test. Other features include specifying a file name for saving data, adjustable sample rate, decimating factor for reducing data recorded, and gain control. All coding is accomplished on the block diagram. While there is a considerable amount of coding an important command is the DAQ Assistant that allows the measurement cards to be adjusted in the ways previously mentioned.

2.5 Material Characterization

Two types of aluminum were tested for this work. The first was 5083-H116 aluminum (Al). It has a strong history of application in naval situations due to corrosion resistance. The second was 6061-T651 Al. This material was selected as a substitute for the more common 6082 aluminum that is more frequently used outside of the United States. The 6061-T651 Al selected is an ideal substitute due to its similarities in composition and strength properties.

2.5.1 5083 – H116 Aluminum

5083-H116 Al, or simply 5083, has a long history of naval applications due to its ability to resist corrosion. Examining the 5083's temper designation, H116, helps to explain the process for making this material. The H designation indicates a strain-hardened wrought product **[27]**. Strain-hardening is performed by cold working the material, meaning it is not hardened with any kind of heat treatment. The 116 designation indicates that it is a specially fabricated material for a corrosion resistant aluminum-magnesium alloy.

Other components of the material include its chemical composition, Table 2-1, and annealing temperature, 413°C **[28]**. The chemical compositions of the material are rough estimates of a typical material and do not necessarily reflect the exact composition of the materials used as a part of this research

Table 2-1: Composition of a typical 5083-H116 aluminum

	Aluminum (Al)	Magnesium (Mg)	Manganese (Mn)	Silicon (Si)	Iron (Fe)	Chromium (Cr)	Zinc (Zn)	Titanium (Ti)	Copper (Cu)
Wt. %	92.4 – 95.6	4 – 4.9	0.4 - 1	Max 0.4	Max 0.4	0.05 – 0.25	Max 0.25	Max 0.15	Max 0.1

2.5.2 6061 – T651 Aluminum

6061-T651 Al, or 6061, is another aluminum that has a history of naval application. T in the T651 temper refers to a thermally heat-treated procedure. The 6 refers to a solution heat treatment with artificial aging, and the 51 indicates a plate whose stress was relieved by stretching the material. Considering all this information indicates that the 6061 material was solution heat-treated at 529°C, stretched to a controlled amount to relieve stress, and artificially aged at 160°C **[29, 30]**.

As done with the 5083, the chemical composition of a typical 6061 is examined. This composition is for a typical 6061-T651 material and does not reflect the exact composition of the material used in this work.

Table 2-2: Composition of a typical 6061-T651 aluminum

	Aluminum (Al)	Magnesium (Mg)	Silicon (Si)	Iron (Fe)	Copper (Cu)	Chromium (Cr)	Zinc (Zn)	Manganese (Mn)	Titanium (Ti)
Wt. %	95.8 – 98.6	0.8 – 1.2	0.4 – 0.8	Max 0.7	0.15 – 0.4	0.04 – 0.35	Max 0.25	Max 0.15	Max 0.15

2.6 Testing Procedure

Testing procedures are key to providing consistency between testing. Steps were taken to ensure that all tests were organized and ran in the same manner leaving as little variability as possible. The procedures for creep and tensile tests are identical up to the point of running the test, so the initial steps discussed apply to all testing.

Before even touching the MTS load frame, calipers are used to measure the thickness and width of the sample and recorded in a spreadsheet. Moving to the load frame, the first steps in the testing procedure are gripping and aligning the sample. A bracket was attached to the upper grip to position the sample in the grips. This made the rest of the alignment process easier. A small level helped to vertically align the sample before gripping the bottom actuator in load control. When gripped in load control, there is some weight on the sample. The load is adjusted to zero pounds. Using the laser-sighting tool, the pyrometer is then aligned to the middle of the sample.

After the alignment is completed, the heating process can be started. First the coils of the induction heater are moved into place around the sample so heating can occur. Labview is then started to record the thermal expansion as heating occurs. Using the PID controller, the desired testing temperature is set and heated at a rate of 50°C/min. While heating occurs, the sample remains at a zero load condition. After the sample reaches testing temperature, it remains untouched for 10 minutes. This will allow any microstructural changes to occur and provide time for the sample to be thoroughly heated. Also, once the testing temperature is reached, a picture of the temperature profile and sample image are taken.

The steps up to this point apply to all testing. From this point on, the procedure varies between tensile and creep testing. Tensile testing procedures are covered first. At this point the sample has been aligned, heated, and has stayed at temperature for 10mins in load control. All tensile testing was completed at a strain rate of 10^{-3} s^{-1}. To run a test with a strain rate, the MTS load frame was changed from load control to stroke control. After switching to stroke control and keeping the load as close to zero as possible, the test is started. Labview records the data and the IR camera records a video of the test. The strain rate was applied until failure after which the data acquisition and video are stopped and the induction heater cooled.

As already mentioned, creep testing has a slightly different procedure than the tensile test. Again, at this point the sample has been aligned, heated, and held at its testing temperature for 10mins. For a creep test, a load is applied and remains until the sample fails. The load for a test was determined by multiplying the desired stress by the area of the sample. Loading was done at 200lbfs/s until the load corresponding to the stress was reached. From that point on the load was monitored to ensure there was no change until the sample failed. Data was recorded in Labview as the sample remained loaded until failure occurred. If a load was selected that did not fail in a reasonable amount of time, approximately 2hrs, the test was stopped. Upon completion, the sample was cooled and removed and the process repeated for the rest of the tests.

CHAPTER 3 – Elevated Temperature Tensile Test Results

3.1 Introduction

As talked about multiple times already, these materials have specific application as aluminums used to construct naval ships. Specifically important is their response to fire on ships. Elevated temperature mechanical testing is the easiest way to measure strength properties of both materials at a variety of temperatures.

3.2 Testing Matrix

Since elevated temperature is a vague statement a testing matrix was developed to organize and narrow down the areas of interest. A summary of all the tests done for the 5083 and 6061 are summarized in Table 3-1.

Table 3-1: Test matrix for elevated temperature tensile testing

	5083-H116		6061-T651	
Temperature (°C)	Mechanical Extensometer	Laser Extensometer	Mechanical Extensometer	Laser Extensometer
25 (RT)	3	1	3	1
50	3	1	3	1
100	3	1	3	1
150	3	1	3	1
200	3	1	3	1
250	3	1	3	1
300	3	1	3	1
350	3	1	3	1
400	3	1	3	1
450	3	1	3	1
500	3	1	3	1

Information from Aerospace Specification Metal (ASM) provides a solidus and liquidus temperatures of 591 and 638°C for 5083 and 582 and 652°C for 6061 respectively **[28, 30]**. To keep from getting too close to those temperatures, 500°C was selected as the maximum temperature for testing. From there tests were done in increments of 50°C to fully capture the degradation of mechanical properties as the temperature increases.

Multiple repetitions were done for each temperature to not only to confirm strength property results, but to also provide a standard error associated with their calculation. That is why a combination of the laser and standard extensometers was used in the testing. This will show agreeability between the two devices and help with fully

characterizing the material. While the standard extensometer can only measure up to 50%, the laser extensometer can measure beyond that and show a full stress-strain curve from loading until failure.

3.3 Test Results and Analysis

Seen in the test matrix, Table 3-1, a number of mechanical tests were performed over a large variety of temperatures. Before getting to far into tests and results a comparison was done at room temperature for the standard and laser extensometers. After confirming consistency and repeatability of tests, the rest of the temperatures were tested and the resulting stress-strain curves were recorded.

3.3.1 Laser and Mechanical Extensometer Comparison

Before going into testing all the different materials, two tests were done at room temperature for the 6061 Al. One test was performed using the mechanical extensometer and the other using the laser extensometer. Two results were expected from these tests. There is consistency between using different styles of extensometers and consistency with the resulting stress-strain curves. The two experimental setups are shown in Figure 3-1.

(a) **(b)**

Figure 3-1: Test setup with mechanical and lasers extensometer

Figure 3-1a, uses the mechanical extensometer, with the induction heater, pyrometer, and IR camera. The shelf on the front of the load frame is used to hold the laser extensometer, Figure 3-1b. Also with the laser extensometer the IR camera is moved to the back of the machine. Using these two test setups gave the following result for room temperature tensile tests.

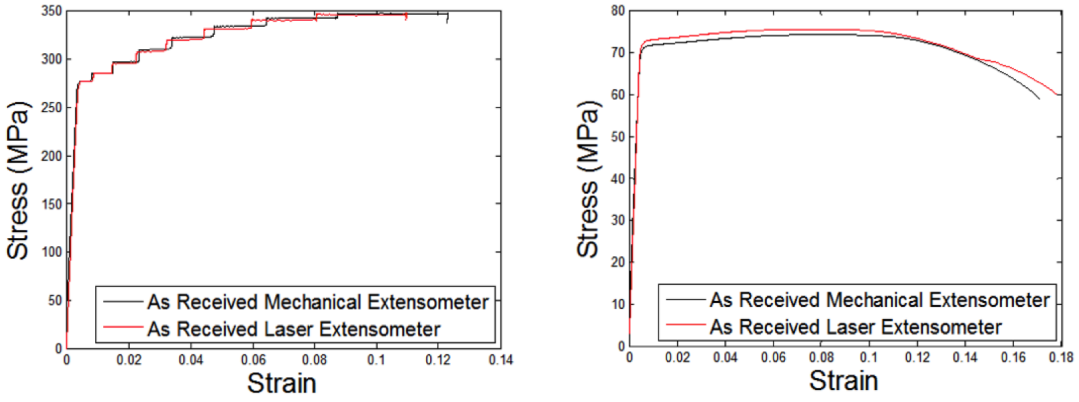

Figure 3-2: Comparison of as received room temperature tests using mechanical and laser extensometers

Results from the room temperature test, Figure 3-2, look very promising. Looking a little closer at the curves shows almost identical elastic regions as well as the transition to the plastic region. Very minor discrepancies are noticeable, but are easily accounted for due to the small differences between samples and where failure occurs in relation to the measurement equipment.

Knowing that both extensometers can be trusted for testing and produce repeatable results, testing at elevated temperatures can be completed with confidence.

3.3.2 Elevated Temperature Tensile Testing 5083-H116 Results

Following the test matrix outlined in Table 3-1, elevated temperature tensile testing was completed on the 5083 material. The mechanical and laser extensometers were both used as a part of this testing showing both consistency and accuracy for all tests. Showing how well the two measurement techniques line up is Figure 3-3 that shows the as received room temperature tests.

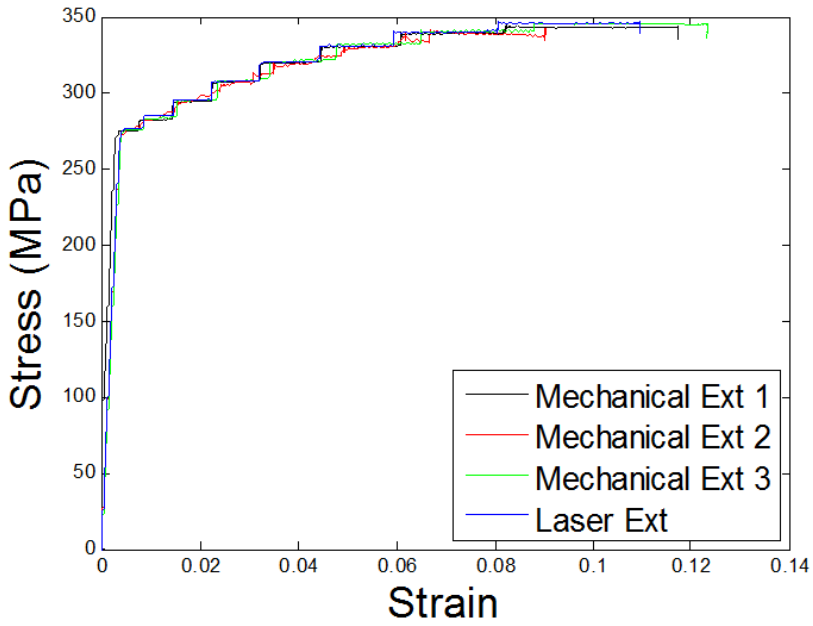

Figure 3-3: As received room temperature tests for 5083 Al using mechanical and laser extensometers

Tests AR-5083tensile-01, 02, and 03 were completed using the mechanical extensometer and test AR-5083tensile-04 utilized the laser extensometer. These four tests fall on top of each other showing that consistency between multiple tests and instruments.

Going beyond the room temperature testing, the same process was used for all elevated temperature tests, three mechanical extensometer tests and one laser extensometer. Following the procedure outlined in Chapter 2.6, the results of the 5083 elevated temperature tensile tests are displayed in Figure 3-4.

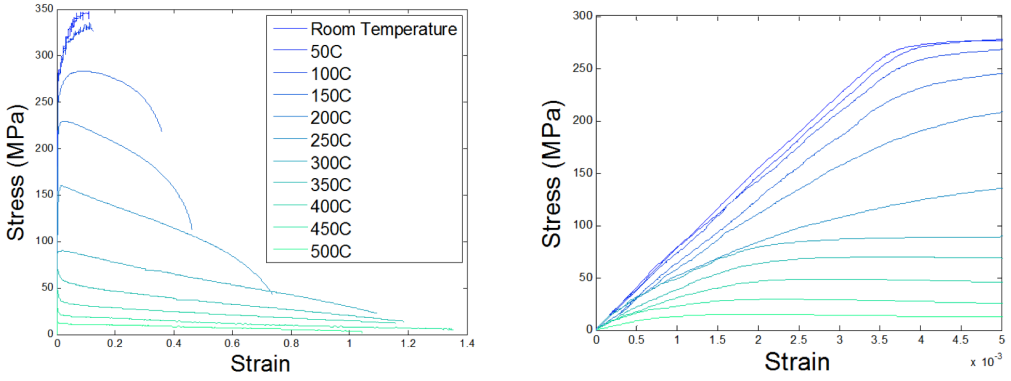

Figure 3-4: Stress-strain curves for 5083 Al

In Figure 3-4a, there are a couple features that stand out. First is the decrease in strength properties, specifically yield and ultimate strength, between the temperatures of 200 to 350°C. A trend of decreasing strength is expected as the material gets hotter and is quickly confirmed from Figure 3-4b that shows the elastic regions.

Another aspect of the plot is the overall trend of increasing strain at failure, expect for 500°C where the strain is less than the lower temperatures. An examination of the at the failed specimens illustrated in Figure 3-5 also displays this characteristic.

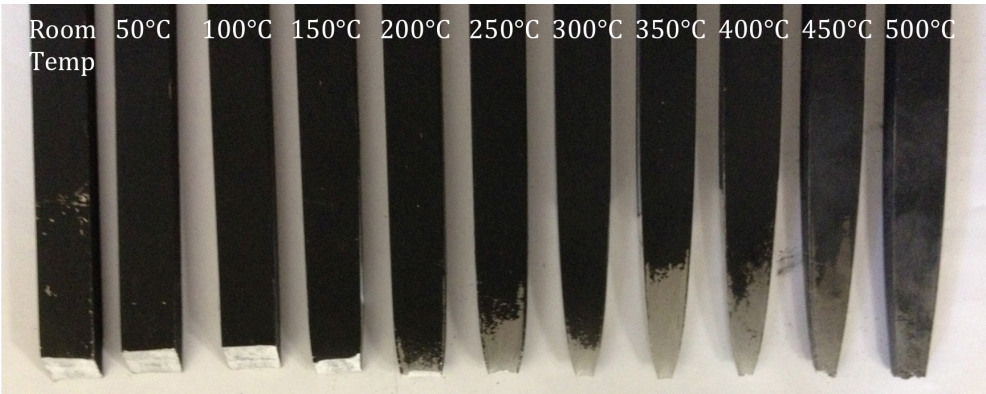

Figure 3-5: Failed samples for 5083 Al

Ductile shear failure is present in the material up to 100°C, after which the material becomes more ductile up to 400°C. At temperatures above 400°C there does not appear any particular failure mode as the samples appear to be so weak they just melt apart. Relating back to Figure 3-4, the elongation of the samples corresponds what is seen with the strain at failure. The overall increasing trend, except at 500°C where the elongation is not as substantial confirms the second observation of Figure 3-4.

While the couple observations made from Figure 3-4 are useful for obtaining a high-level understanding of the materials, it is still better to go beyond the lines and try to comprehend what the numbers say about the material. Before going to that phase there is one other interesting feature specific to 5083. Again looking back at Figure 3-4 the room temperature, 50 and 100°C stress-strain curves don't seem to look as smooth as the other tests. This is because of an effect known as the Portevin-Le Châtelier (PLC) effect that is present in aluminum-mangenese alloys **[31]**. Shown in Figure 3-6, the PLC effect is seen with the strain hardening behavior at room temperature and 50°C and a lesser extent at 100°C

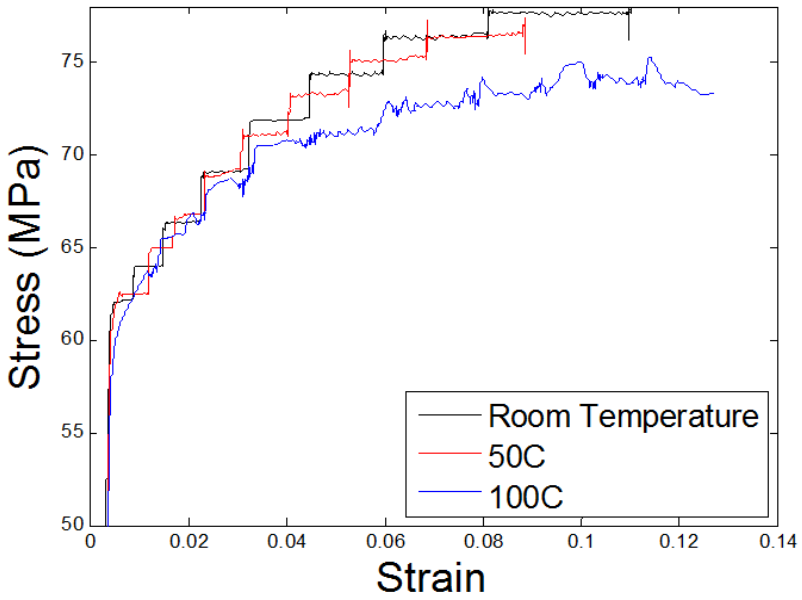

Figure 3-6: 5083 Al tests showing Portevin-Le Châtelier effect

This effect is known to be due to the presence of manganese solute atoms in the material. Interaction between these manganese solute atoms and mobile dislocations in material are one possible reason behind this effect **[32]**. Moving to the other end of the spectrum, 350°C and hotter, a different kind of behavior is observed.

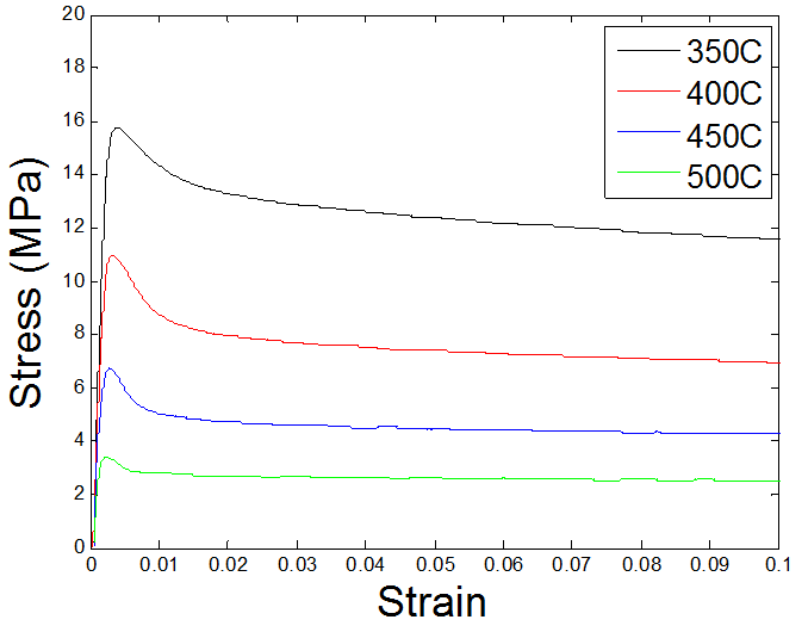

Figure 3-7: 5083 Al tests showing material softening after yielding

While the lower temperatures experienced a hardening effect, the higher temperatures experience a softening effect. After getting past the elastic region into

plastic strain, the material experiences a quick release of stress before slowly necking and eventually failing.

3.3.3 Elevated Temperature Tensile Testing 5083-H116 Analysis

Making high-level observations by looking at the stress-strain curves is a quick way to get an understanding of the material. However, to really understand the behavior of the 5083 under high temperature conditions, going beyond the curves is required. Some aspects that will be examined here include elastic modulus, yield strength, ultimate strength, and reduction of area as a function of temperature. All of the numerical values for these properties are summarized in Appendix A.

Elastic modulus is the first property examined subsequent to the tension testing. The elastic modulus is a measure of the stiffness of the material and is defined as the slope of the elastic region of the stress-strain curve. Instead of reporting each value from the testing, the four moduli values calculated for each temperature were averaged together and shown in Figure 3-8 as a single point with error bars, where the error bars represent the error in repeatability of the tests.

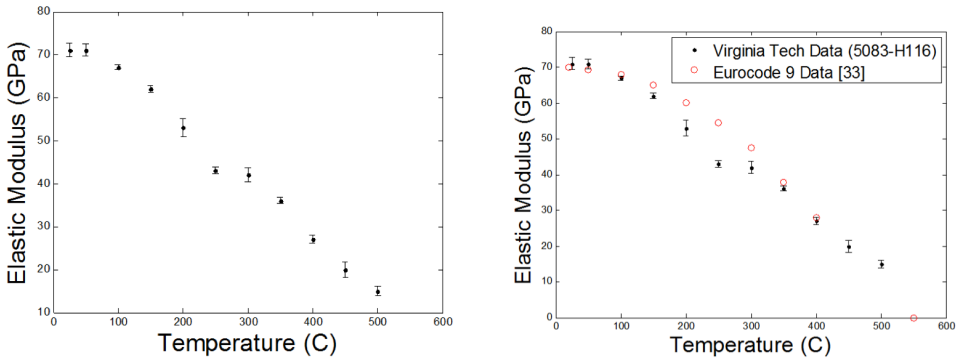

(a) (b)

Figure 3-8: Elastic Modulus vs. temperature for 5083 Al

Two curves are shown here, Figure 3-8 shows just the results from the high temperature testing and Figure 3-8 is the same set of data compared to results taken from tests completed in the publication of the British Standard Eurocode 9 **[33]**.

Before look at the comparison, a couple features of the test results will be examined. The first key feature is the consistency of moduli values from room temperature to 50°C. A minimal change would be expected at this point along the temperature scale. 25°C is the difference of temperature between the two tests, which compared to the full scale of temperature is very small and why there is no significant difference between the two modulus values. The second key feature is the overall trend of a linearly decreasing elastic modulus with temperature. This indicates a steady decline in the stiffness of the material as temperature increases, which again is what would be expected with the increasing temperature. The only temperature that stands out from this trend occurs at 250°C where the stiffness appears to temporarily plateau. 250°C is an

interesting temperature in aluminum. At this point, microstructural failures are changing causing precipitates to interact with dislocation walls causing some behavior like this to occur.

Comparison to the values determined in Eurocode 9 is very good. The low and high temperature moduli are almost identical while Eurocode 9 predicts slightly higher, but no unreasonable values through the mid-range of temperatures. Discrepancies could be explained by the lack of material defined in Eurocode 9. Values measured there are said to be common to all aluminums, but as seen from this testing is not always the case.

Yield strength is the next strength property to examine. It is defined as the stress at which the transition occurs from elastic to plastic strain, and the material starts to take on permanent deformation. Using a similar procedure to that used for the elastic modulus, the 0.02% offset yield strength was calculated for each test and then the four values averaged for each temperature. Figure 3-9 shows the results for the yield strength.

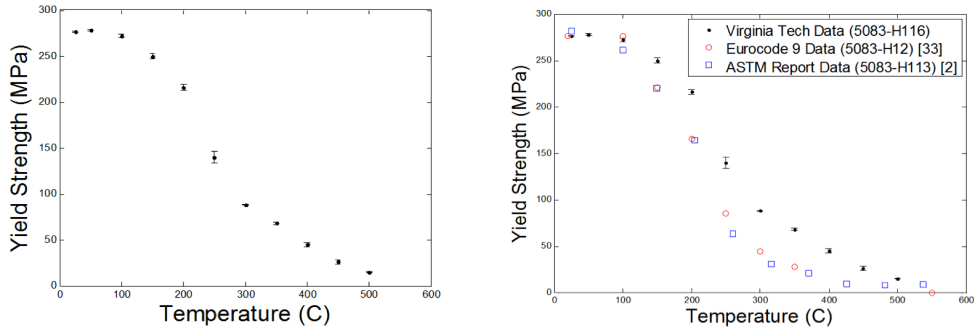

Figure 3-9: Yield strength vs. temperature for 5083 Al

Unlike the linear degradation of elastic modulus, yield strength declines in regions. Region one occurs between room temperature and 150°C. Over this region the strength remains relatively constant. A decrease in strength starts to become noticeable at 150°C which leads into the second region. This region lasts from 150 to 300°C. Over this temperature range, the strength dramatically decreases from 250 to 88MPa. This region corresponds to the plateau seen in the elastic modulus where precipitate and dislocation wall interaction is causing a substantial weakening of the material. Moving past this point, the final region occurs between 300 and 500°C. At this point the microstructure has been severely damaged and the yield strength exhibits a linear decline.

Results from Eurocode 9 and an ASTM report of elevated temperature properties of aluminum were used as a comparison to the yield strength values. The lower temperature line up very well between all the sources, but there are some discrepancies at the higher temperatures. From the data collected in this work, the higher temperatures linearly decline in strength while the other sources show a rapid decline in stress around 250°C and leveling out as the temperature approaches 500°C. Even though the approach to these points is different the resulting final strengths are almost identical in value.

After looking at elastic modulus and yield strength, the final strength property to examine is the ultimate strength. Ultimate strength is the maximum strength that occurs during the tensile test and defines the point where the onset of necking occurs. As done with the other tests, the ultimate strength was determined for each test and averaged by temperature to show the results in Figure 3-10.

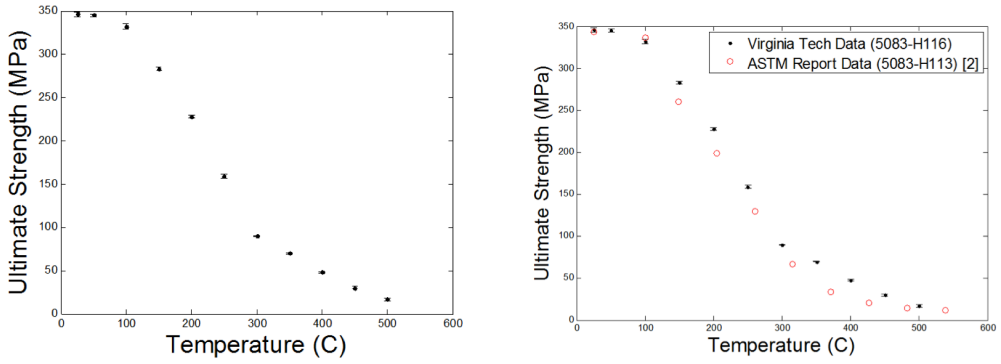

Figure 3-10: Ultimate strength vs. temperature for 5083 Al

If the behavior of the ultimate strength looks familiar, it is because the behavior is very similar to the yield strength. As is the case, the same regions used for the yield strength will be examined for the ultimate strength. The first region spans from room temperature to 150°C. Strength of this region starts constant, but starts to decline at 150°C. This change corresponds to the PLC effect discussed in Figure 3-6. At this point the strain hardening behavior ends and the ultimate strength occurs closer to the yield strength rather than right before failure. From 150 to 300°C shows the same effect as the yield strength. The strength of the material rapidly declines with the increasing temperature changing from a strength of 283 to 90MPa. Going from 300 to 500°C is characterized by a linear decline in strength to a value of 17MPa.

A comparison of data was made with data published in the ASTM report on aluminum properties. There is not much to saw about this comparison because the two data sets are nearly identical. The only real minor difference is strength from the ASTM report declines slightly faster than the data recorded in this work.

Ultimate strength concludes the measurement of strength properties, but one more measurement was completed to find the reduction of area. Reduction of area is a characterization of the ductility of the sample and the change of values will match the changes occurring in Figure 3-5.

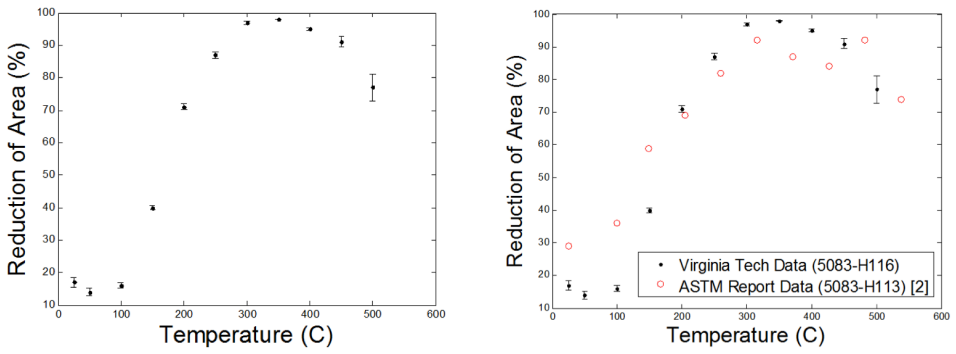

(a) (b)

Figure 3-11: Reduction of area vs. temperature for 5083 Al

Reduction of area measurements really helps to quantify the behavior seen in Figure 3-5. From room temperature to 100°C the failure is a ductile shear with very little change in reduction of area values. The failure of the sample then becomes more and more ductile losing the shear behavior of the low temperatures. This occurs from 100 to 350°C corresponding to the increasing values of the reduction of area. Reduction of area values then start to decrease between 350 and 500°C. This corresponds to a transition from ductile to brittle failure. Once this transition to brittle failure occurs, the material starts to lose ductility as seen by the decreasing reduction of area measurements.

Using the ASTM report on aluminum, a comparison was made to the data measured in this work. Once again there is good agreement between the two sources. The lower temperatures vary a little in numerical values, but they show a similar trend. Reduction of area starts off constant, increases to a peak value around 350°C then decrease with the transition to brittle failure.

3.3.4 Elevated Temperature Tensile Testing 6061-T651 Results

The process taken with the 5083 Al was done with the 6061 Al. In accordance with the test matrix, Table 3-1, three tests were completed with the mechanical extensometer and one was done with the laser extensometer in increments of 50°C from room temperature to 500°C. Using room temperature tests as an example, Figure 3-12 shows the repeatability of the tensile tests.

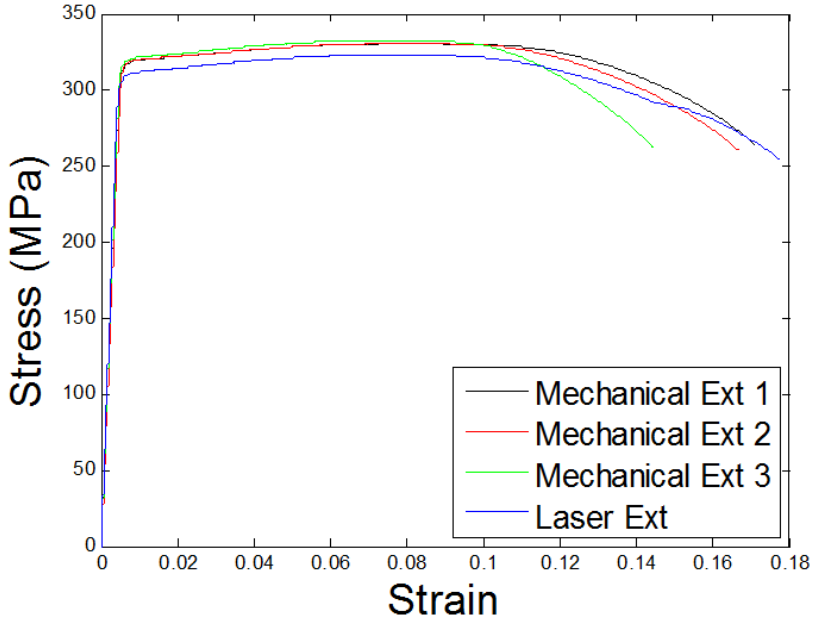

Figure 3-12: As received room temperature tests for 6061 Al using mechanical and laser extensometers

Similar to the results of Figure 3-2, consistency within the elastic and plastic regions up to ultimate strength is observed. Knowing that 6061 also has the consistency seen in the 5083, all of the curves can be plotted together so trends can be seen over the whole range of temperatures.

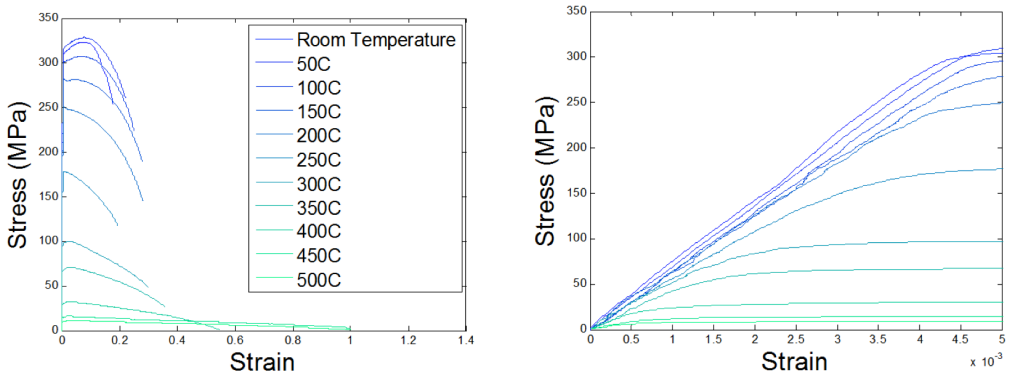

(a) (b)

Figure 3-13: Stress-strain curves for 6061 Al

There are a couple of features that stand out in Figure 3-13. The first thing that stands out is how each curve is lower than the previous indicating a decrease in mechanical properties with increasing temperature. Also seen is the increasing trend of strain at failure with temperature. This behavior can also be observed by examining the failed samples as shown in Figure 3-14.

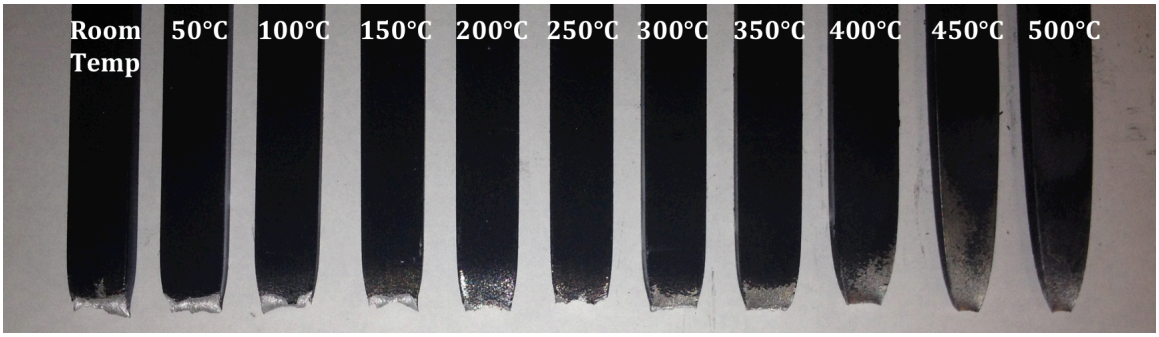

Figure 3-14: Failed samples for 6061 Al

Ductile fracture is the dominant method of failure that becomes more and more ductile with increasing temperature. Figure 3-14 shows agreement with Figure 3-13 in respect to elongation and strain at failure. Overall there appears to be no surprises with the tensile testing. Intuitively everything makes sense looking solely at the stress-strain curves.

3.3.5 Elevated Temperature Tensile Testing 6061-T651 Analysis

As was done with the 5083 material, it is beneficial to go beyond the curves to the actual numerical results of the testing. Properties of elastic modulus, yield strength, ultimate strength, and reduction of area were observed as a function of temperature to characterize the behavior of the material. Appendix A also has the numerical values for the mechanical properties discussed in this section.

Looking first at the elastic modulus will give an indication of how soft the material becomes as the temperature increases. These properties were determined by measuring multiple points along the elastic region of the stress-strain curve. After the points were determined they were fitted with a linear regression with the resulting slope the value for the elastic modulus. Since four tests were completed for each temperature the value displayed is an average of the tests with a standard error due to repeatability.

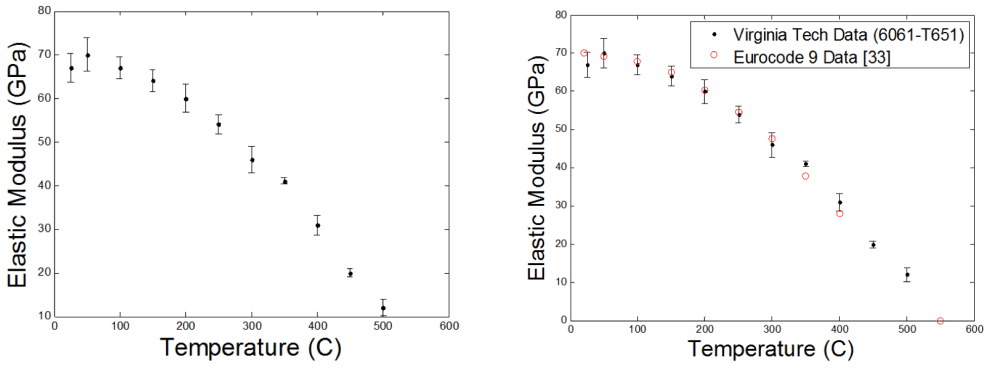

Figure 3-15: Elastic modulus vs. temperature for 6061 Al

Breaking down Figure 3-15 into sections will help with the understanding of what is occurring. The first section is from room temperature to 100°C. In this region there is almost no change in the elastic modulus. Being relatively low temperatures, it makes sense that stiffness would not change any substantial amount. Moving on to higher temperatures in the range of 100 to 350°C, there starts a noticeable drop in stiffness. The actual value of elastic modulus changes from 67 to 41GPa. It is after this point where the stiffness really starts to degrade. From 350 to 500°C the elastic modulus values drops from 41 to 12GPa. In this range of temperatures the material becomes very soft and will yield under a small amount of stress.

The next step is to then compare these results to other literature values. Values determined as part of Eurocode 9 are used for this comparison. These published values are essentially an identical match to the testing results. A note about the Eurocode results is there is no material associated with the results. Values used are fairly standard for all aluminums so there is no particular material designation for the data.

After observing the impact temperature has on the stiffness of the material, yield stress will be examined next. Yield strength is an important property to know because it defines the upper limit to which a load can be applied before permanent deformation occurs. Calculations were done for each tensile test by determining the 0.02% offset yield stress and averaging the values.

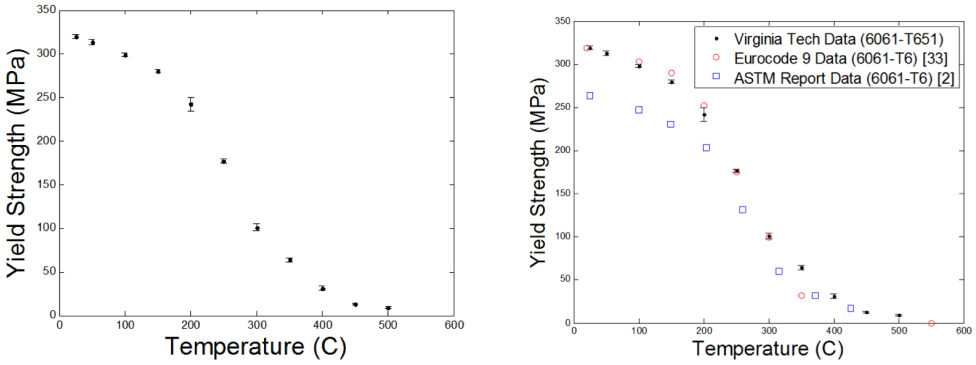

(a) (b)

Figure 3-16: Yield strength vs. temperature for 6061 Al

Again, breaking Figure 3-16 down into temperature regions will help see what is occurring with the yield strength as a function of the increasing temperature. The first section is the region from room temperature to 150°C. In this region the strength steadily declines from 319 to 242MPa. While a noticeable drop-off in strength, it is minimal compared to the next region. Between 150 and 400°C, the yield strength of the material degrades at a much quicker rate with the largest drops occurring between 200 and 300°C where the yield strength drops from 242 to 101MPa. At this point it was already determined that the material is no longer stiff and now its observed that the yield strength is about 1/3 of its original strength. The final region from 400 to 500°C doesn't have any

significant change in yield strength because it has essentially reached 0. A strength of 9MPa is all that remains at 500°C, approximately 3% of the room temperature strength.

Comparisons were once again made to the data, and for this strength results from Eurocode 9 and an ASTM report on aluminum mechanical properties were utilized. Results from Eurocode 9 appear to agree very well with those from this work. For the ASTM report, the high temperature yield strengths appear to agree, but the low temperatures do not. One possible explanation for the difference could be the preparation of the material. The 6061 samples tested in the ASTM report were an extrusion while the 6061 samples used in this work were from a plate. Difference in the forming process could account for differences in yield strength.

The last strength property that will be examined is ultimate strength. Ultimate strength is the largest stress that can occur before the onset of necking. This strength is determined by finding the maximum value of stress that occurs during the tensile test. As with the other strengths, the value was calculated for each test and averaged with the other tests of the same temperature. The results of the ultimate strength are shown in Figure 3-17.

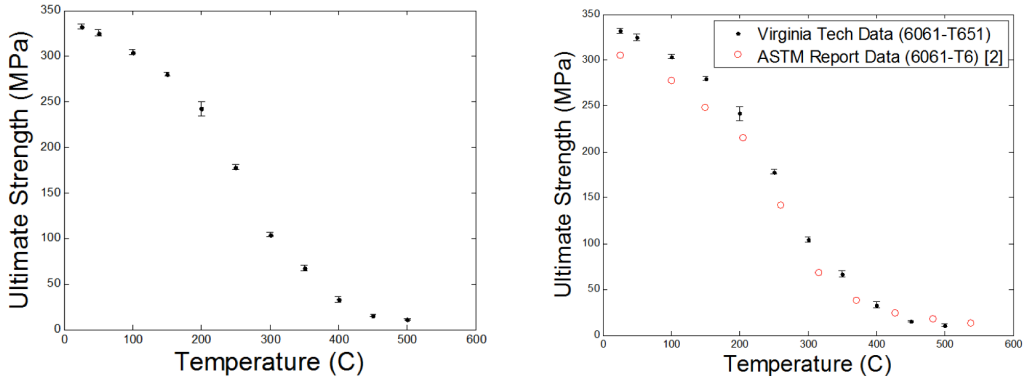

Figure 3-17: Ultimate strength vs. temperature for 6061 Al

At first glance, Figure 3-17 appears to be identical to Figure 3-16. In one respect the two figures show the same behavior occurring, but their values and meaning are slightly different. Since the ultimate strength behaves in a similar fashion to the yield strength, it will be broken down into the same regions. From room temperature to 150°C shows the steady decline in ultimate strength from 332 to 280MPa. While this is a noticeable decrease in strength it is minimal compared to the change occurring from 150 to 400°C. Like the yield strength, the material loses all strength as the ultimate strength drops from 280 to 33MPa with the largest drop-off occurring between 200 and 300°C. Upon reaching 400°C the material has almost no strength left as the ultimate strength is 10% of its original value. At this point most of the damage has occurred as the ultimate strength in the final region, from 400 to 500°C, drops from 33 to 11MPa.

Unlike the previous two strengths, ultimate strength is only compared to the ASTM report. Just like all the previous other measurements, the results from the literature line up very well with the measured results. In the same manner as the yield strength, the ASTM report has matches up well with the high temperatures, but has smaller values for the low temperatures. However, the difference is not significant enough to warrant anything other than a small mention.

Reduction of area was measured as a means of understanding ductility and elongation of the sample as a function of temperature. Before each sample was tested, the width and thickness were measured using calipers. The samples were then heated and failed following the procedure outlined in Chapter 2.6. After which the width and thickness of the failed region were measured again. The reduction of area was then calculated as the percent difference between the two measurements. After these calculations are completed the results are shown in Figure 3-18.

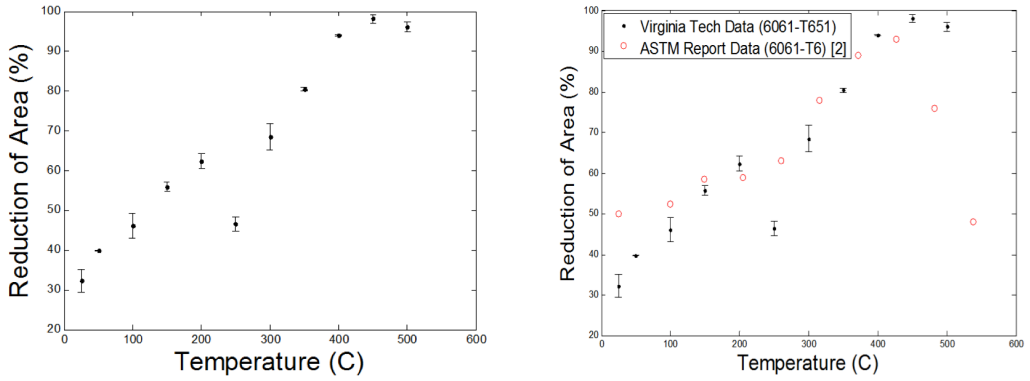

(a) (b)

Figure 3-18: Percent reduction of area vs. temperature for 6061 Al

In the same manner that the elastic modulus decreases with temperature, the reduction of area increases. There is an overall trend of a relatively linear increasing ductility expect for two points, 250 and 500°C. 250°C is an interesting transition period in the microstructure where precipitates and dislocation walls are interacting in a manner that is causing the material to be less ductile. At 500°C the failure of the material has transitioned from a ductile failure to a brittle one. As also seen in the 5083 to a greater extent, the brittle failure mechanism also causes a decrease in ductility.

A comparison to reduction of area measurements from the ASTM report confirms these results. Around 210°C there is a drop in reduction of area, but the change is not as substantial as the tests done with this work. However, on the high temperature end the same trend of decreasing ductility is present, but the ASTM report show a much larger decline than measured in the testing.

CHAPTER 4 – Creep Test Results

4.1 Introduction

With the conclusion of the tensile testing the next step is to move on to creep testing. Creep testing is defined by a test in which a known load is applied to a fixed sample and left there for a certain period of time or until failure occurs. While there are testing machines specifically designed for creep testing, this work will utilize the same MTS machine used for tensile testing, Figure 3-1, and follow the procedure outlined in Chapter 2.6.

4.2 Test Matrix

As was done with the tensile tests a test matrix was developed that utilized both the mechanical and laser extensometers. When developing this test matrix, both temperature and stress were considered. The goal was to test a variety of temperatures with multiple stress levels per temperature. Table 4-1 is the result of this planning.

Table 4-1: Test matrix for elevated temperature creep testing

	5083-H116			6061-T651	
Temperature-Stress	Mechanical Extensometer	Laser Extensometer	Temperature-Stress	Mechanical Extensometer	Laser Extensometer
200-160	1	2	200-220	1	2
200-140	1	2	200-210	1	2
200-120	1	2	200-200	1	2
250-100	1	1	250-150	1	1
250-80	1	1	250-140	1	1
250-60	1	1	250-130	1	1
300-50	1	2	300-80	1	2
300-40	1	2	300-70	1	2
300-35	1	2	300-60	1	2
350-30	0	2	350-50	1	1
350-25	0	2	350-45	1	1
350-20	0	2	350-40	1	1
400-18	0	3	400-20	1	2
400-15	0	3	400-15	1	2
400-13	0	3	400-13	1	2

Testing was done with temperatures ranging from 200 to 400°C with stresses from 220 to 13MPa. These ranges were chosen to provide a big picture representation of the creep behavior for both materials. Some things that stand out as differences between the two materials are the stresses selected to test at. Due to the higher yield strength of the 6061, higher stresses were used to try and match the time and response of 5083 creep tests. Another note is the mechanical extensometer was not used for the 350 and 400°C tests for 5083. This was because the elongation was so substantial at these temperatures that mechanical extensometer was not able to capture enough of the strain behavior.

4.3 Test Results and Analysis

Unlike the tensile testing, the creep testing was a much longer process. Instead of a defined strain rate, stresses were selected so most tests would take anywhere between 10min to 90min. Careful attention was paid to make sure all stresses selected were less than the yield strength for a given temperature and failed within a reasonable amount of time, no more than 3hrs. Upon conclusion of the test, measurements were made to determine the steady-state strain rate that would in turn become the inputs for creep modeling.

Three regions, primary, secondary, and tertiary, define a typical creep curve. The primary stage is first seen at the start of a creep test and is characterized by a slow increase in strain as the load takes the material through the elastic region and into plastic deformation. Secondary creep is the next region and typically lasts most of the test. This section known by its linearly increasing strain, and is also the region where the steady-state creep rate is determined from. Once the material starts to neck and approach failure, the material enters the tertiary region. Here the strain rapidly increases as the material becomes weaker and eventually fails. These regions are shown and labeled in Figure 4-1.

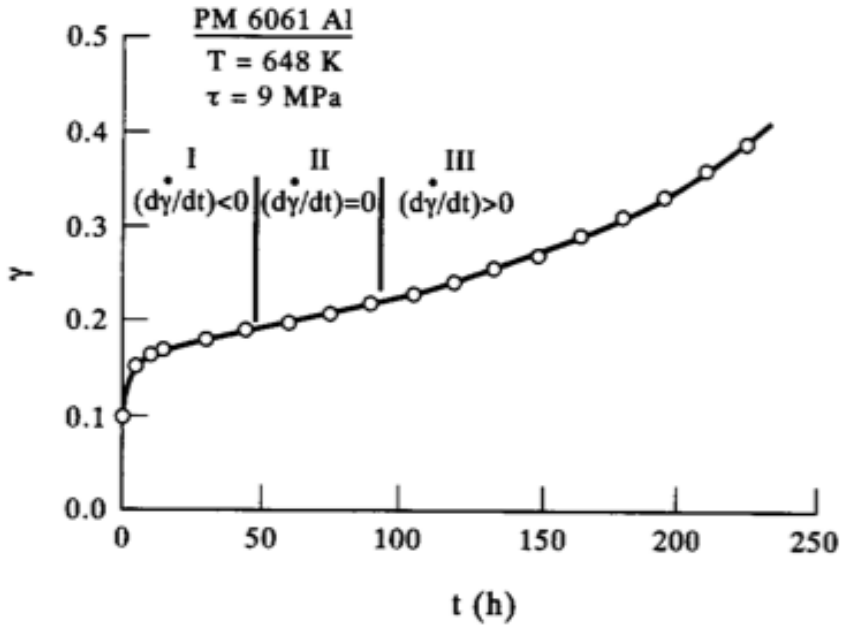

Figure 4-1: Primary, secondary, tertiary creep regions [18]

The 5083 and 6061 tested for this work both exhibit clear secondary and tertiary regions. In the 5083, a small primary region can be seen, and in the 6061 the primary region is so small that it is not noticeable in the curve.

4.3.1 Creep Testing 5083-H116 Results

Referring back to Table 4-1 shows what tests were done for 5083. At the 100's, 200, 300, and 400°C, three tests were done while two tests were done at the 50's, 250 and

350°C. Following the procedure described in Chapter 2.6, each test involved heating the sample to its testing temperature, letting it sit for 10min, and then applying a load determined by the stress and area of the sample. Unlike the tensile tests, strain measurements were the only desired output from the test. Load and temperature were also monitored to insure conditions did not change during the test.

For a typical creep test the results will look like something shown in Figure 4-2.

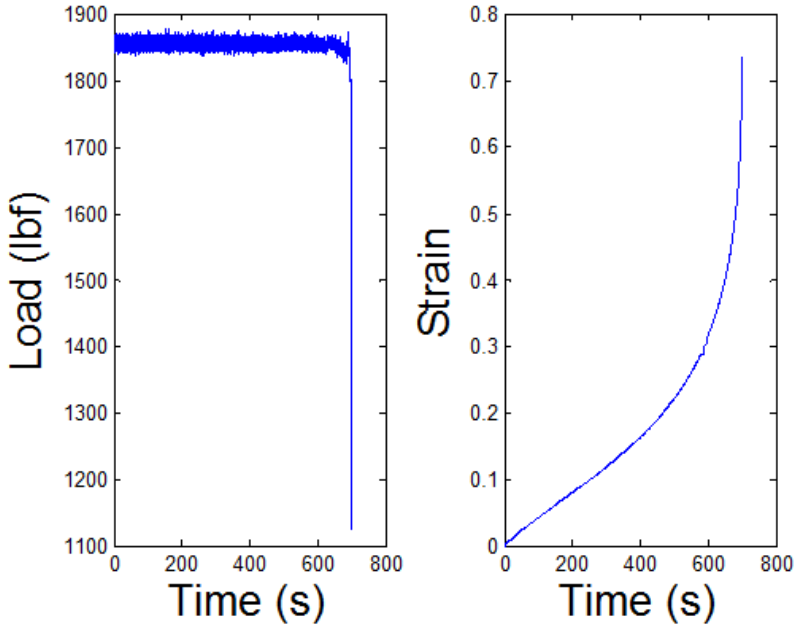

Figure 4-2: Load-time and creep strain-time plots for 250°C and 100MPa

Load is applied as close to instantaneous as possible and held constant until the sample is about to fail at which time the load slowly then quickly drops off as the sample is no longer able to maintain the original load. On the strain side, there is a small primary region that occurs over approximately the first 50 seconds. The secondary creep region follows the primary from 50 to 400 seconds then turns to tertiary creep until failure. For the most part the 5083 will follow this behavior, but with each test exhibiting slightly different times for each region.

From this point forward each temperature will be examined showing only the strain-time curves for every test done at that temperature. The first temperature tested was 200°C. At this temperature 3 tests were completed at stresses of 160, 140, and 120MPa.

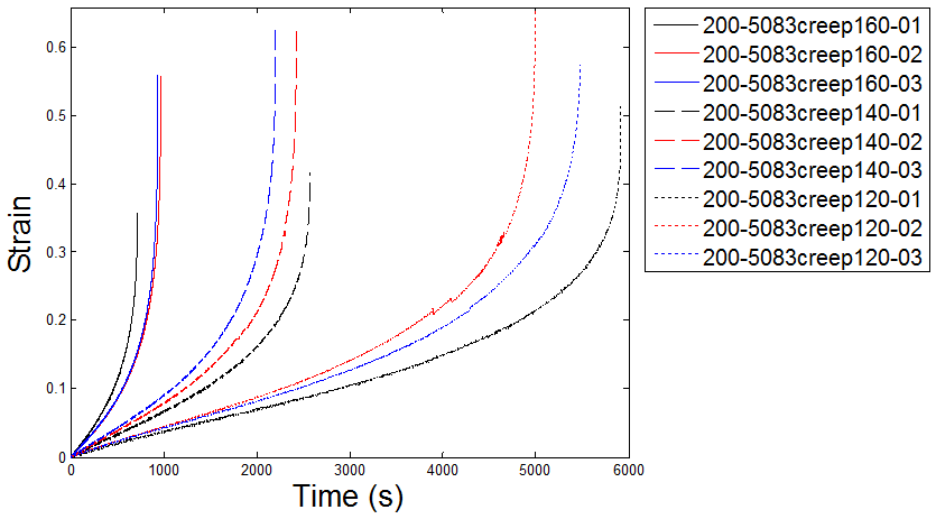

Figure 4-3: Creep strain-time curves for 200°C creep tests at 160, 140, and 120MPa

As shown in Figure 4-2, there is a small primary, secondary, and tertiary region also seen in Figure 4-3. Before looking at the curves the legend needs to be explained to understand what each means. The first number is the testing temperature, in this case 200°C. The next section describes the material tested, 5083, the type of test, creep, and the stress tested at, 160, 140, or 120MPa. The final number is the test iteration, test 1,2, or 3.

Moving on to examining the curves shows three distinct areas that correspond to the three stresses. Within each stress there is some variability between each test. This could be due to a couple reasons. There could be some variations in temperature that could cause some difference, or variability in sample geometry causes failure to occur faster or slower, or there is just some natural variability in the material.

Going on to the other temperatures will show a similar pattern in creep regions, separation of stress, and variability between tests. 250°C was the next testing temperature. At this temperature tests were completed at 100, 80, and 60MPa. The decrease in stress was done to keep stress below the yield strength at this temperature and try to have testing times similar to that of 200°C

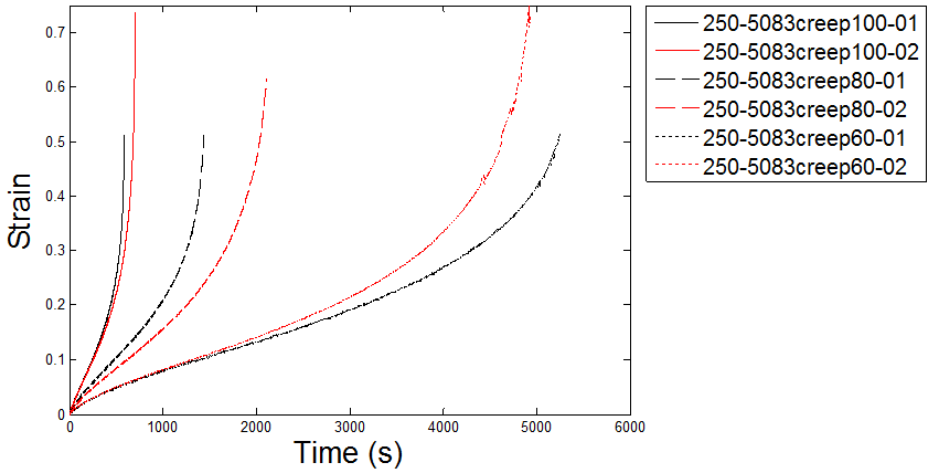

Figure 4-4: Creep strain-time curves for 250°C creep tests at 100, 80, and 60MPa

Stated in the test matrix, only two iterations were completed for this temperature. Again there is a small primary region followed by a secondary and tertiary region. There is also the three distinct stress regions with the same variability seen in the 200°C tests.

Tests at the other temperatures, 300, 350 and 400°C, show the same behaviors previously mentioned for the 200 and 250°C tests. Figure 4-5, Figure 4-6, and Figure 4-7 show the remaining creep tests for 5083.

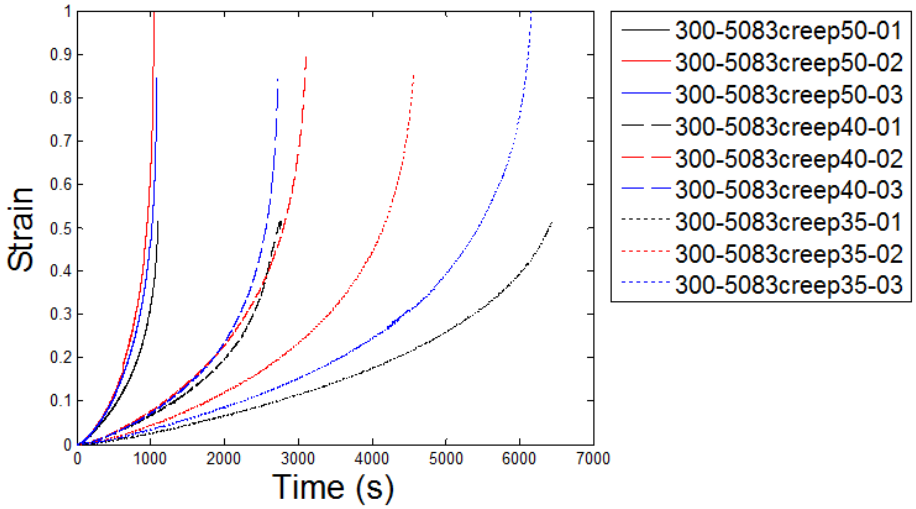

Figure 4-5: Creep strain-time curves for 300°C creep tests at 50, 40, and 35MPa

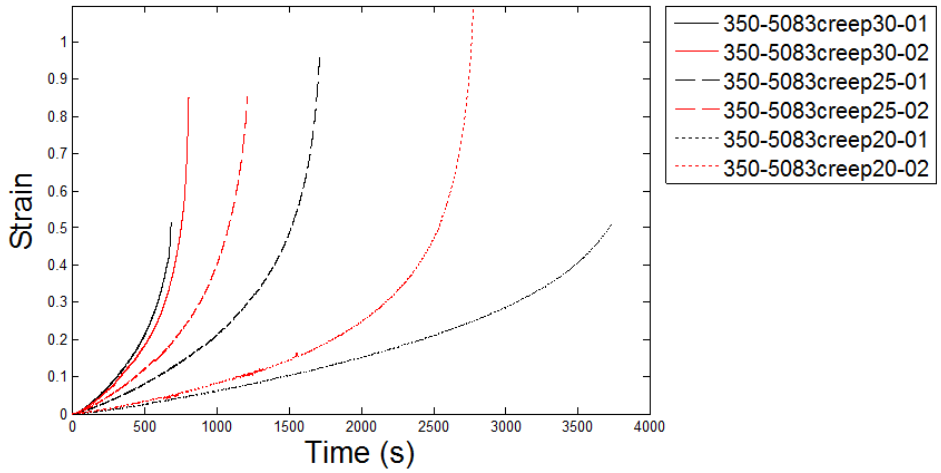

Figure 4-6: Creep strain-time curves for 350°C creep tests at 30, 25, 20MPa

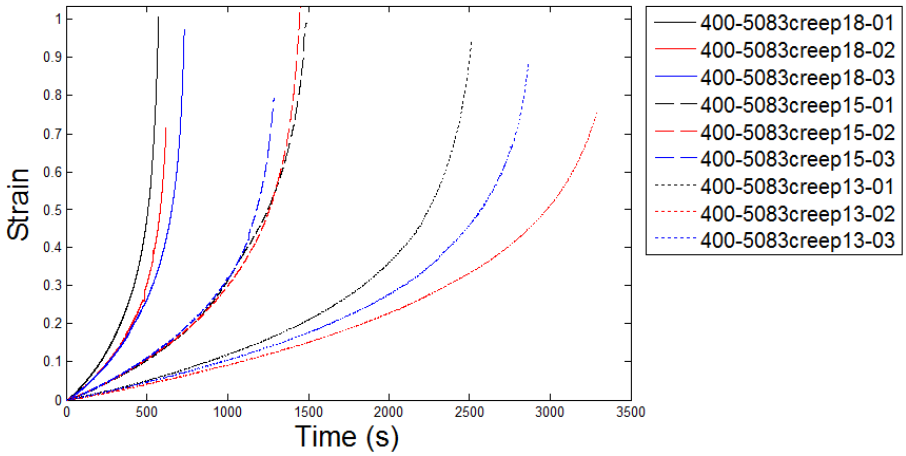

Figure 4-7: Creep strain-time curves for 400°C creep tests at 18, 15, 13MPa

Without being too repetitive the same patterns clearly stand out in theses tests as well; distinct groups of stresses with variability in each group. The only difference is the lack of a noticeable primary region. The temperatures just reached a point where the material has softened enough that the occurrence of a primary region is so small that it cannot be seen in the figures.

4.3.2 Creep Testing 5083-H116 Analysis

With the completion of the actual tests, the next step is to analyze the data and extract the necessary information that will be important to creep modeling. Analyses of the creep test include looking at aspects such as steady-state strain rate and effects of temperature and stress on the material.

One of the first steps upon completion of a creep test is calculating the steady-state strain rate. The slope of the linear secondary region defines steady-state strain rate.

A section of the secondary region is selected then, using a program like Excel or Matlab, the slope is calculated by fitting a linear line to the data. An example of this process, done in Matlab, is shown in Figure 4-8.

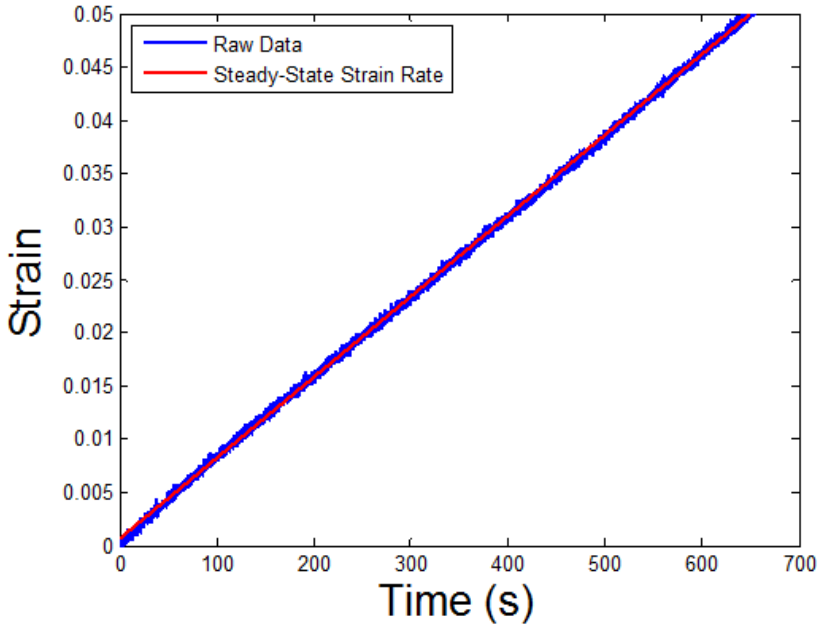

Figure 4-8: Steady-state strain rate calculation for 5083 Al 200°C 140MPa creep test

For this example the creep test was completed at 200°C at a 140MPa stress. A section from the secondary region was isolated from the rest of the graph and a linear line fitted to the data. The slope of the fit provided the strain rate, which for this test was $7.585\times10^{-5}s^{-1}$. As a double check to make sure the strain rate value is correct, it was also calculated using Microsoft Excel. Using Excel yielded a value of $7.586\times10^{-5}s^{-1}$. Identical strain rate values confirm that either method is reasonable and can now be completed for all the other creep tests. Figure 4-9 shows the result of these calculations for all the tests completed in Figure 4-3 through Figure 4-7, and Appendix B contains all the numerical values.

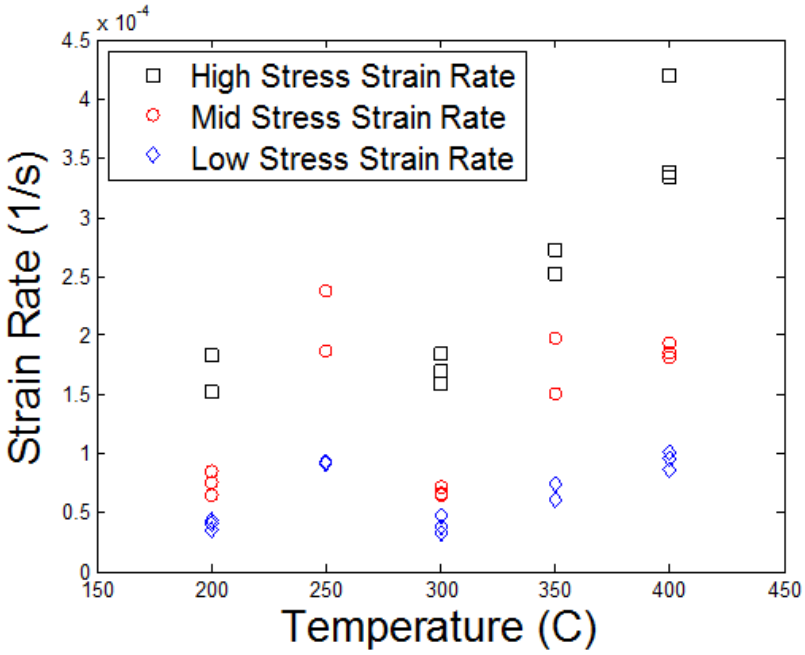

Figure 4-9: Strain rate vs. temperature for 5083 Al

Like the creep curves, the strain rates depict three distinctive regions that correspond to the highest, middle, and lowest stress for a given temperature. Figure 4-9 also shows the variability seen in the creep curves.

Strain rate is a crucial value for creep modeling, but it doesn't fully describe the effect that temperature and stress play on the material. Looking back over Figure 4-3 through Figure 4-7, there aren't any stresses repeated across temperatures meaning each temperature uses three stresses that are not used at another temperature. This is partially dictated by the decreasing yield strength, but also due to the sensitivity of the material to different loadings at elevated temperatures. Looking closely at the time to failure shows that each temperature follows a similar pattern. The highest stress fails between 10 and 20min, the middle stress fails between 30 and 40min, and the lowest stress fails between 1 and 2hrs. To illustrate how this difference an example using 100MPa will be described. At 200°C the next stress that would be tested, following the pattern, would be 100MPa. Following the relationship established by the other tests, 100MPa at 200°C would take 2hrs at a minimum, most likely longer to fail. However, increasing the temperature to 250°C has a completely different effect. 250°C and 100MPa tests were completed and took only 10mins. This is a substantial difference and clearly illustrates how temperature and stress can play a large effect on creep testing.

4.3.3 Creep Testing 6061-T651 Results

After going through the 5083 creep results a couple of things were learned. There exists a small primary region followed by clear secondary and tertiary regions, variation is a factor for each stress-temperature combination, and temperature and stress both play an important role on the reaction of the material. With all of this in mind, the same

aspects will be examined for 6061 seeing what is similar and what is different between the two materials.

Creep testing done on the 6061 was completed over a temperature range from 200 to 400°C and stresses from 13 to 220MPa. Already there is one difference between the materials. To maintain a similar pattern in behavior and failure times, higher stresses were used to compensate for the higher yield strength at the lower temperatures. Moving on to the actual results, the first set of tests were completed at 200°C at stress values of 200, 210, and 220MPa.

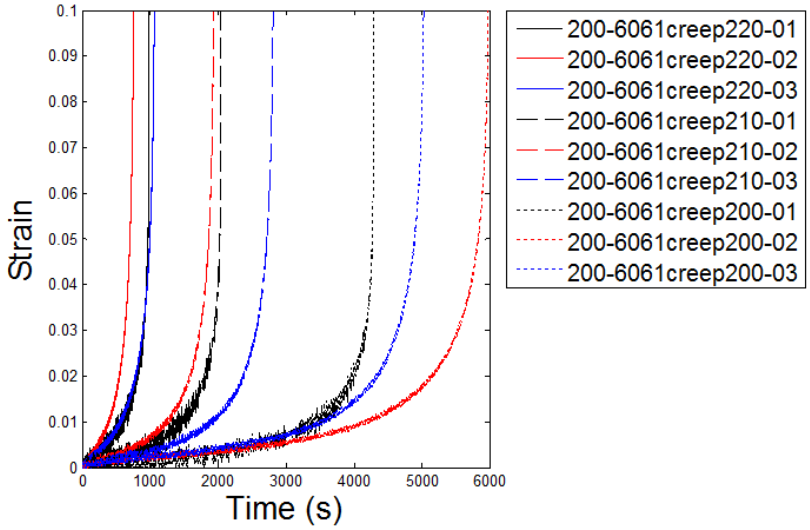

Figure 4-10: Creep strain-time curves for 200°C creep tests at 200, 210, and 220MPa

Even at a quick glance a couple differences already stand out between the two materials. The first difference is the absence of a primary creep region. In the 5083 creep tests a primary region, though small, was present in the curves. For 6061 no such region can be found. If a primary region is present it is so small that it cannot be identified from the data. Another noticeable difference is the shape of the curve. For the 5083 the slope of the secondary region is much greater before transitioning into the tertiary region. Being a less ductile material, the 6061 have a flatter secondary region that quickly becomes tertiary then fails. Differences aside, there are also some similarities between the two materials. The distinctive stress regions and variability within each stress region are still present in the results.

Moving to higher temperatures, as expected, shows a similar behavior to the 200°C creep tests.

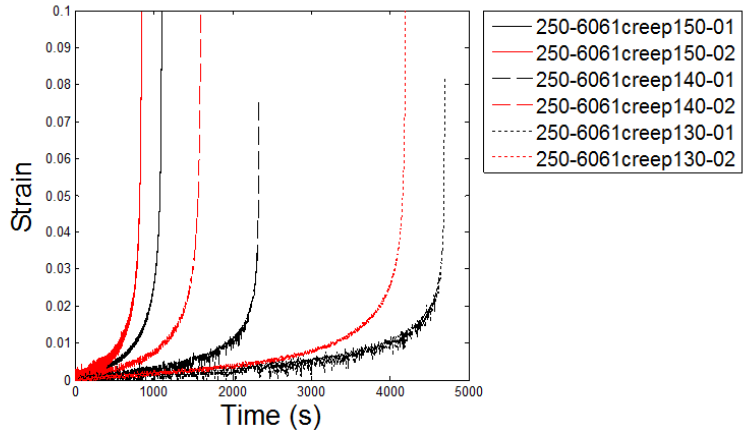

Figure 4-11: Creep strain-time curves for 250°C creep tests at 130, 140, and 150MPa

Figure 4-11 shows the same trend seen in Figure 4-10. No primary region is discernable from the curves, and the three stresses have distinguishable groups with variability. This same behavior can be seen with the rest of the 6061 creep testing.

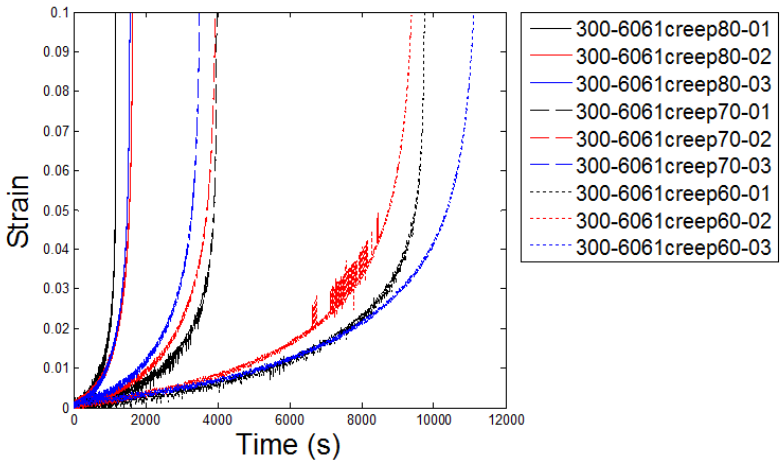

Figure 4-12: Creep strain-time curves for 300°C creep tests at 60, 70, and 80MPa

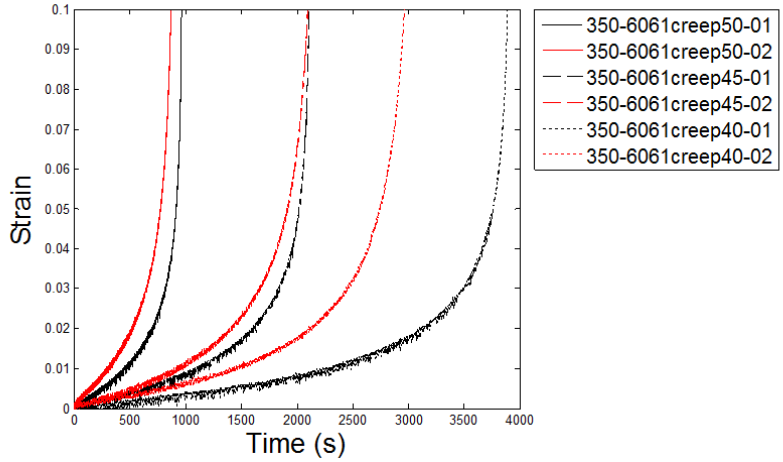

Figure 4-13: Creep strain-time curves for 350°C creep tests at 40, 45, and 50MPa

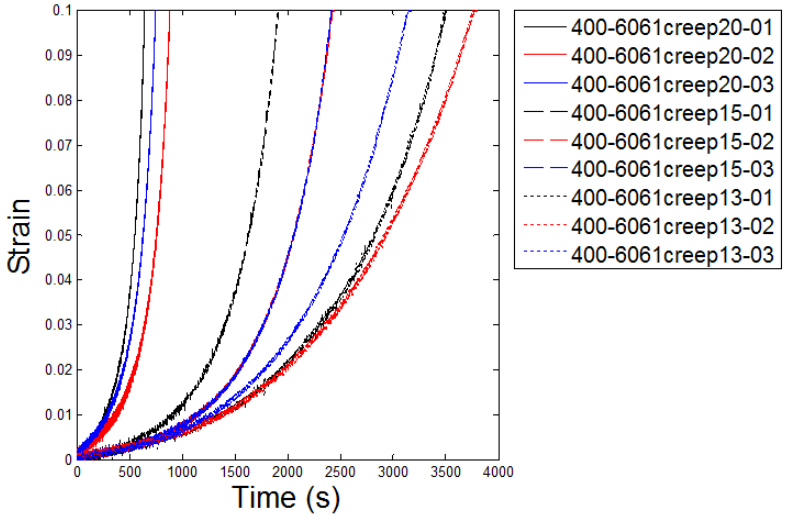

Figure 4-14: Creep strain-time curves for 400°C creep tests at 13, 15, and 20MPa

Like the other tests, Figure 4-12 through Figure 4-14 shows the same behavior and similar results to the previous temperatures for 6061.

4.3.4 Creep Testing 6061-T651 Analysis

Analysis for the 6061 creep tests will be completed in the same fashion as the 5083. The steady-state strain rate will be examined followed by a look at the effects of temperature and stress.

Both Matlab and Excel were used to determine the strain rates. Like the previous tests, a section of the linear secondary region was removed from the data. In Matlab, the data was fitted to a linear regression, and in Excel the slope was calculated from the data points. Figure 4-15 shows a representation of what the region that was fitted would look like.

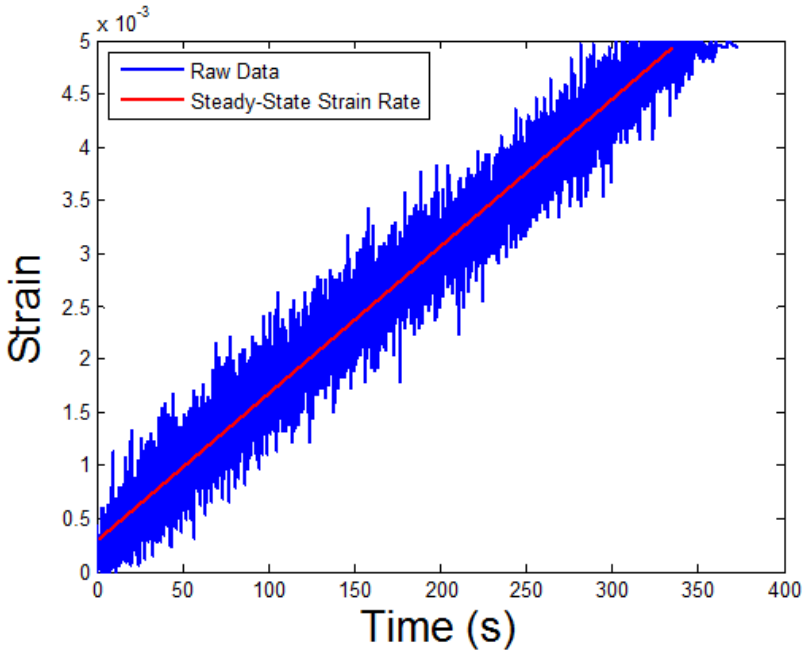

Figure 4-15: Steady-state strain rate calculation for 6061 Al 200°C 210MPa creep test

From this set of data, Matlab determined the strain rate to be $5.712\times10^{-6}s^{-1}$ and Excel returned a value of $5.718\times10^{-6}s^{-1}$. Just like the 5083 test, there is a small, but negligible difference between the two values confirming that once again either method can be trusted to give the strain rate. This process was again repeated for all the tests shown in Figure 4-10 through Figure 4-14. Appendix B also contains a more complete breakdown of the strain rate values calculated for each test. For a visual representation of the strain rates, Figure 4-16 is provided.

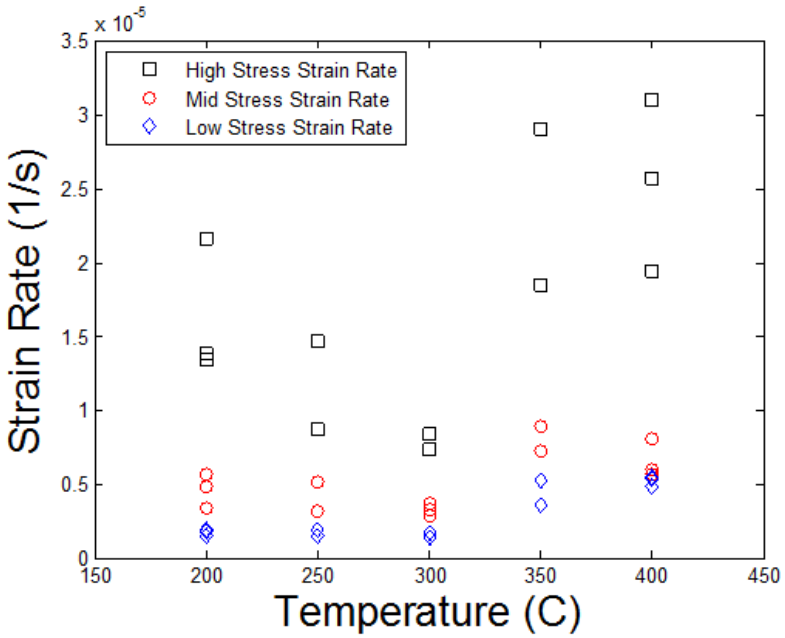

Figure 4-16: Strain rate vs. temperature for 6061 Al

As seen with the data, each temperature shows distinctive groupings of stress, except for 400°C at which stress is so low that the strain rates meld together more than the other temperatures. A noticeable difference from Figure 4-9 is the larger variation of strain rates at each temperature. Factors such as temperature fluctuations and noise in the measurement could account for some of the variation.

The effects of temperature and stress are even more evident for 6061 than 5083. Looking back through the stresses that were tested as a part of the 5083 creep analysis shows constantly decreasing stress values with no large changes. However, the opposite is true for 6061. At 200°C the lowest stress tested was 200MPa. Increasing to 250°C, the highest stress tested was 150MPa. A change in 50MPa over 50°C is a significant difference which would also cause a significant impact on strain rate. At 200°C with a 200MPa stress, the sample would creep for approximately 1hr 20min. A decrease of 50MPa would significantly lower the strain rate and take a substantial amount of time to fail. If the reverse was done and a 200MPa stress was applied at 250°C, the sample would fail before the corresponding load was reached. While temperature and stress are important factors to consider for both materials, the impact has a much larger effect on the 6061.

4.4 Creep Modeling

The creep data by itself is useful to have, but does not provide much help for predictions of other temperature-stress combinations or finite element modeling. To accomplish this task of providing a simpler method for prediction, creep modeling was done to compliment the creep tests. When referring to creep modeling, it means an equation that takes into account temperature and stress and provides a strain rate as its output.

There are a couple of things to first consider before diving straight into creating a creep model. One of the first questions would be what exactly is being modeled. Is it the primary, secondary, or tertiary region? Depending on the region would greatly affect the complexity of the model. Another consideration would be stress being modeled and predicted. Some models could more accurately predict high stresses while some are better for low stresses, and some try to characterize the entire range **[25]**. To model the creep testing completed in this work, secondary creep is the main focus of the model. Three models will be examined, the first is better suited to predict low stress, the second higher stress, and the third encompasses the entire range.

4.4.1 Activation Energy

Before jumping into the actual models, the activation energy needs to be calculated for each material. Activation energy is the energy required for a creep mechanism such gliding or grain boundary diffusion. Two methods can be used to determine activation energy. The first is using Equation 4-1 and the other is a graphical approach.

$$Q = R\frac{ln\left(\frac{\dot{\varepsilon}_1}{\dot{\varepsilon}_2}\right)}{\left(\frac{1}{T_2}-\frac{1}{T_1}\right)} \qquad \text{Equation 4-1}$$

From this equation Q is the activation energy in kJ/mol, R is the universal gas constant of 8.314 J/mol-K, $\dot{\varepsilon}_1$ and $\dot{\varepsilon}_2$ are two strain rate values in s^{-1}, and T_1 and T_2 are temperatures from the corresponding strain rates in K. The one variable that is not seen in this equation is a stress term. To complete this calculation, strain rates and temperatures must be different, but occur at the same stress value. The other method is a graphical approach where the natural log of the strain rate is plotted against the inverse temperature. The points on the plot create a linear line that has a slope of –Q/R. Multiplying the slope by the universal gas constant provides the activation energy. Since there was no repetition of stress in the creep tests, a special test was completed where a load was applied at an initial temperature then ramped 10°C every 10min. For 5083, tests were completed at 120MPa from 150 to 200°C, 60MPa from 200 to 250°C, and 35 from 250 to 300°C, and for 6061 tests were completed at 130MPa from 200 to 250°C and 70MPa from 250 to 300°C. An example of one test is shown in Figure 4-17.

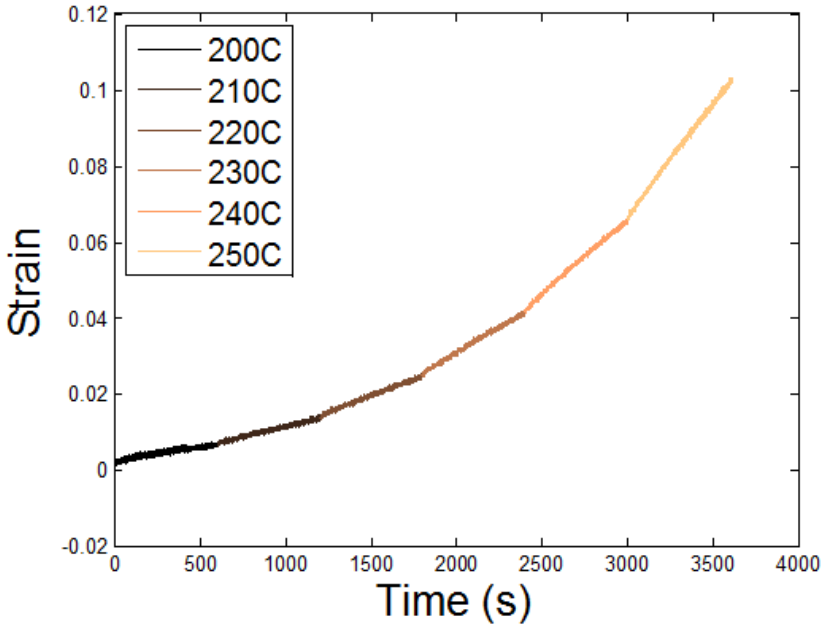

Figure 4-17: Activation energy test for 5083 Al at 60MPa

Shown here with each temperature increase, the strain rate also increases. This type of test was completed for all the previously mentioned scenarios and the strain rates calculated. Upon completion of these tests, the activation energy was calculated in the manner already described.

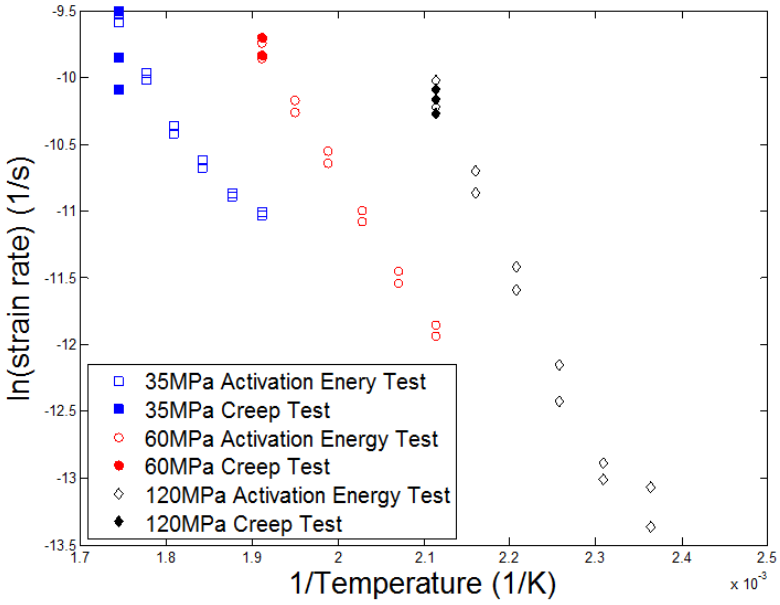

Figure 4-18: Activation energy calculation for 5083 Al

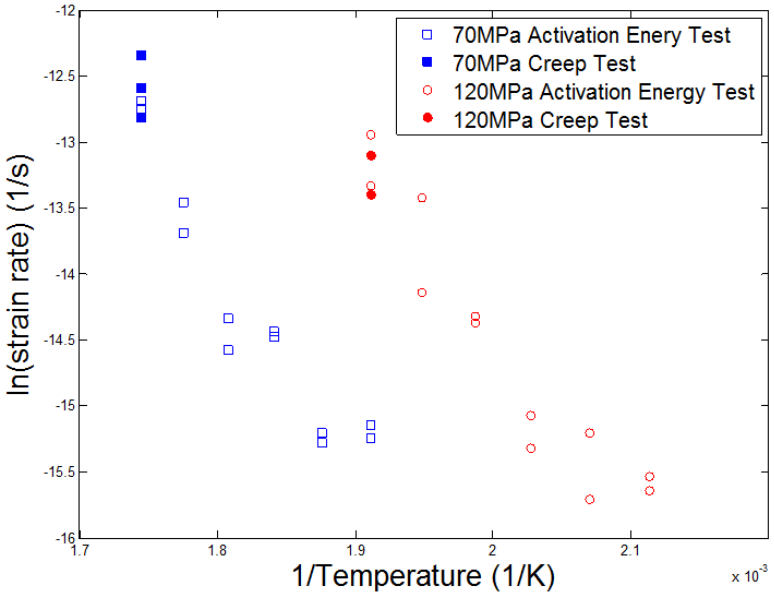

Figure 4-19: Activation energy calculation for 6061 Al

From Figure 4-18 and Figure 4-19, a linear line was fitted to the data and multiplied by the universal gas constant to provide a value for the activation energy of each material. The values for activation energy are summarized in Table 4-2.

Table 4-2: Activation Energy

	5083-H116	6061-T651
Q (kJ/mol)	89	122

While there are multiple curves for each material, the values reported are an average for the two or three tests. Results of creep testing on similar materials by others indicate that the activation energies calculated in this work may be a little low **[24]**. More will be discussed on the matter in Chapter 2.6 under recommendations for future work.

4.4.2 Power Law Creep Model

Proceeding forward with calculated activation energies, creep modeling can be started. The first model to be examined will be the power law creep model. Developed by Dorn, this model generally does better at predicting creep behavior at lower stresses **[21]**.

$$\dot{\varepsilon} = A\sigma^n exp\left(\frac{-Q}{RT}\right) \qquad \text{Equation 4-2}$$

Equation 4-2 is the Dorn power law creep model. Strain rate, $\dot{\varepsilon}$, is the output from the equation in s^{-1}. A ($MPa^{-n}s^{-1}$) and n (unitless) are unknown coefficients, while σ is stress (MPa), Q is activation energy (kJ/mol), R is the universal gas constant of 8.314

J/mol-K, and T is temperature (K). In order to utilize this equation A and n must be solved for. Two methods can be used to determine these variables. The first is to linearize the equation to the form of Equation 4-3 and the second is to use a program like Matlab to do a nonlinear regression on the data.

$$ln(\sigma) = \frac{ln\left(\dot{\varepsilon} exp\left(\frac{Q}{RT}\right)\right) - ln(A)}{n} \qquad \text{Equation 4-3}$$

To simplify notation Equation 4-4 can be substituted in Equation 4-3.

$$Z = \dot{\varepsilon} \exp\left(\frac{Q}{RT}\right) \qquad \text{Equation 4-4}$$

Z is known as the Zener-Holloman parameter and represents a temperature-reduced strain rate. Using this method, a plot can be made that shows $ln(\sigma)$ vs. $ln(Z)$. This results in a graph, Figure 4-20, which can be fitted with a linear equation. The resulting slope and intercept can be used to find values for A and n.

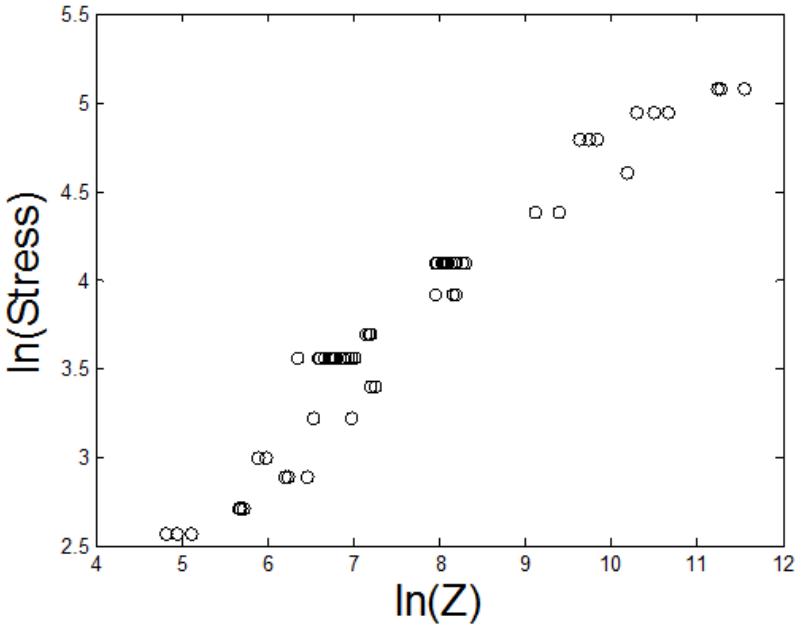

Figure 4-20: Data for power law creep model fitting for 5083 Al

One thing that stands out about this graph is there appears to be a nonlinear aspect at the higher stresses. This is expected to happen since the power law model fits lower stress better. Regardless of true linearity to Figure 4-20, Equation 4-3 was used to find the unknowns, A and n. The other method, nonlinear regression, was also used to find A and n. The process was done for 5083 and 6061 and is summarized in Table 4-3.

Table 4-3: Power law creep model unknowns

	5083-H116		6061-T651	
	A ($MPa^{-n}s^{-1}$)	n	A ($MPa^{-n}s^{-1}$)	n
Linear Regression	0.55	2.70	0.11	3.70
Nonlinear Regression	0.66	2.73	168	1.91

What is clearly evident from the numbers is that both methods provide some difference. To see how significant these differences are, it will be beneficial to use these values to plot Equation 4-2 against the actual creep curves.

Two plots will be created for comparison. The first will be low temperature-high stress and the other will be high temperature-low stress. On each plot the power law creep model using the coefficients determined by the linear and nonlinear regression will model the secondary region.

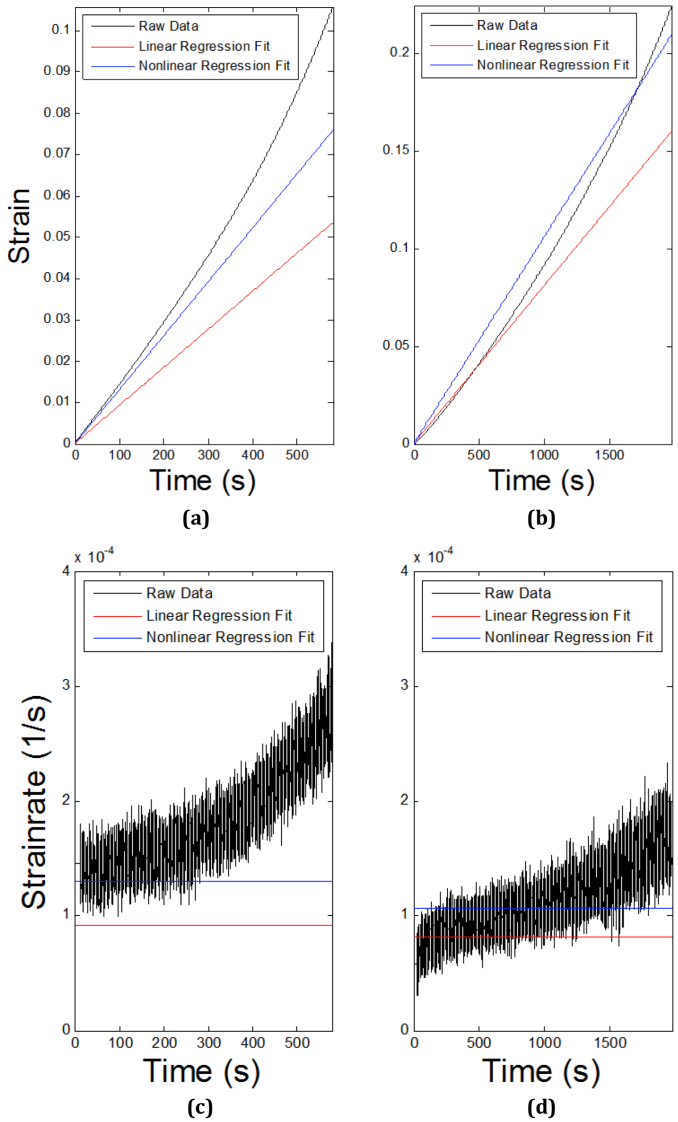

Figure 4-21: Power law model fitted to 5083 Al creep curves

Figure 4-21a,c shows a creep test at 200°C and 160MPa and Figure 4-21b,d is a creep test at 400°C and 13MPa. Plots a and b represents the creep curve with a fitting based on the parameters, and plots c and d show the strain rate against time from the respective curves. The lines on these plots are the calculated strain rates from Equation 4-2. Looking first at the high stress prediction, the power law model under predicts the secondary region of the creep curve. At the low stress, the constants from the linear regression do a good job of predicting the secondary region, but the nonlinear constants over predict the secondary region.

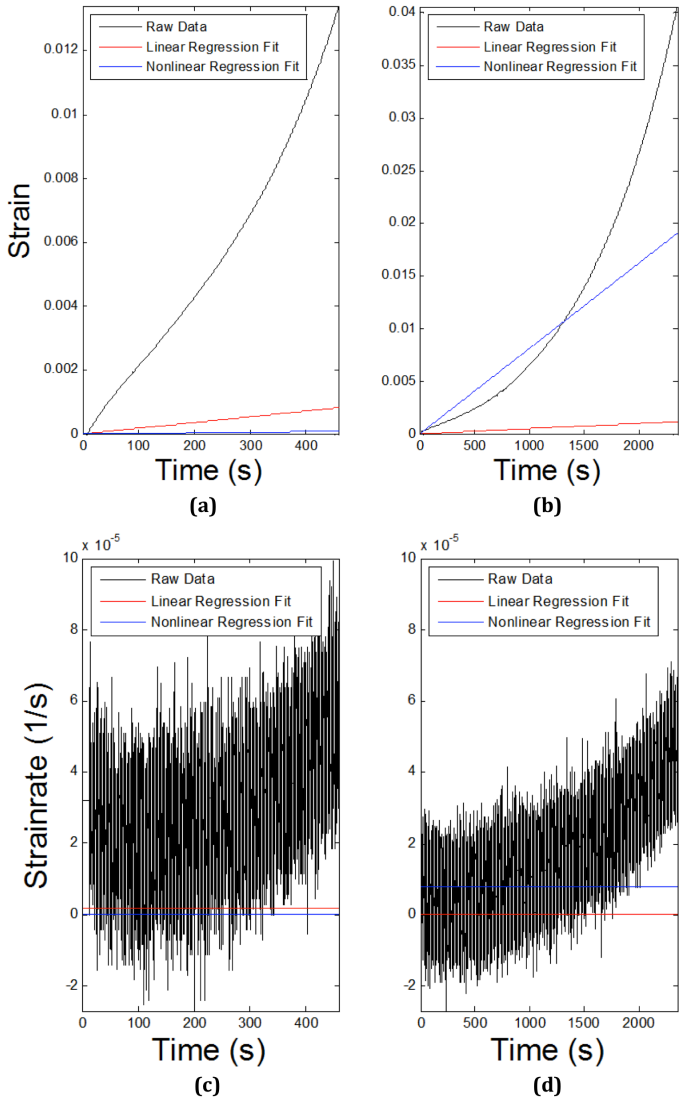

Figure 4-22: Power law model fitted to 6061 Al creep curves

Figure 4-22a,c uses the constants from the linear and nonlinear regressions to predict a 200°C 220MPa creep curve and Figure 4-22b,d predicts a 400°C 13MPa creep curve. The high stress prediction clearly under predicts the secondary region, which was expected due to the low stress accuracy of the model. On the low stress side, the nonlinear model constants do a better job predicting the secondary region, but still slightly miss the mark.

To conclude the power law model, predictions can be made for creep curves, but there accuracy is questionable. High stress cannot be accurately predicted while some success is made with low stress. Each material has some variation with prediction accuracy, but the overall theme is power law is not a very good model for high and low stress creep modeling.

4.4.3 Exponential Creep Model

While the power law was expected to predict low stress, the exponential model is expected to fit higher stresses. Also proposed by Dorn, this model uses the same principal as the power law model with temperature and stress as inputs and strain rate as the output **[21]**.

$$\dot{\varepsilon} = Bexp(\beta\sigma)exp\left(\frac{-Q}{RT}\right) \qquad \text{Equation 4-5}$$

In Equation 4-5, B (s^{-1}) and β (MPa^{-1}) and unknown constants and the other variable are the same as defined in Equation 4-2. From this equation, the same two approaches were used to find the unknowns. Linearizing the equation has the form shown in Equation 4-6.

$$\sigma = \frac{ln\left(\dot{\varepsilon}exp\left(\frac{Q}{RT}\right)\right) - ln(B)}{\beta} \qquad \text{Equation 4-6}$$

Comparing to the linearized power law equation, Equation 4-3, the only difference is the stress term where the power law has a natural log and the exponential equation does not. By plotting stress, σ, against the Zener-Holloman parameter, Equation 4-4, and fitting a linear curve to the data will provide the unknowns B and β.

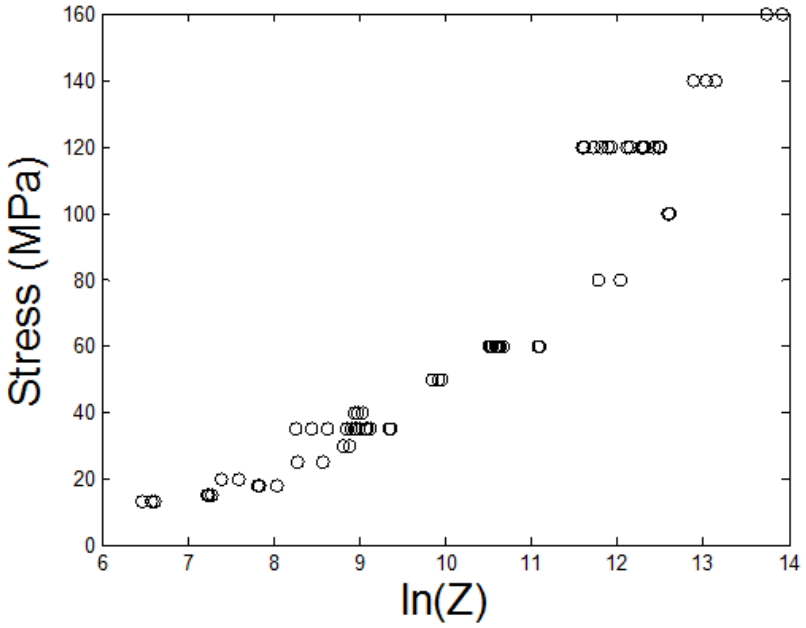

Figure 4-23: Data for exponential law creep model fitting for 5083 Al

In the opposite manner of the power law model, Figure 4-23 has a linear portion at the high stress values, but not at the low stress. This nonlinearity will make the data significantly harder to fit and will show up when trying to compare to the creep curves.

The other method was the nonlinear regression completed using Matlab. The nonlinear regression works by taking inputs of known variables, a nonlinear equation, and initial guesses for the unknown variable and trying to find values for the unknowns that best match the output. For creep modeling the known variables include temperature, stress, activation energy, and universal gas constant. Initial guesses for the unknown variables are determined by using the values calculated as part of the linear regression. Using all theses inputs, Matlab will try to determine the best values for B and β that best match the steady-state strain rates. The result of these two methods is summarized in Table 4-4.

Table 4-4: Exponential law creep model unknowns

	5083-H116		6061-T651	
	B (s^{-1})	β (MPa^{-1})	B (s^{-1})	β (MPa^{-1})
Linear Regression	1.22×10^{3}	0.047	1.22×10^{4}	0.045
Nonlinear Regression	982	0.046	1.93×10^{4}	0.045

In the same manner done with the power law, these variables are put back into Equation 4-5 and used to predict the steady-state strain rate for high and low stress creep tests.

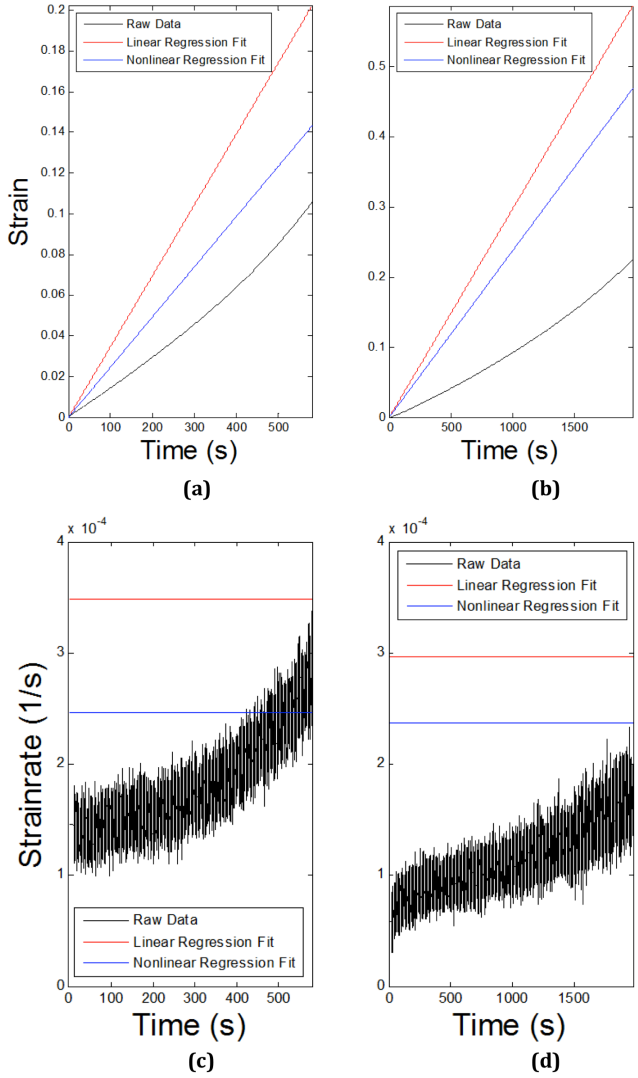

Figure 4-24: Exponential law model fitted to 5083 Al creep curves

The exponential model does not do a very good job of fitting either of the creep curves. Figure 4-24a,c is a curve for 200°C 160MPa creep test, and Figure 4-24b,d is from a 400°C 13MPa creep test. Using either the coefficients from the linear or nonlinear regression give similarly bad results. The one note is that the exponential model is a slightly better fit to the higher stress test, which would be expected.

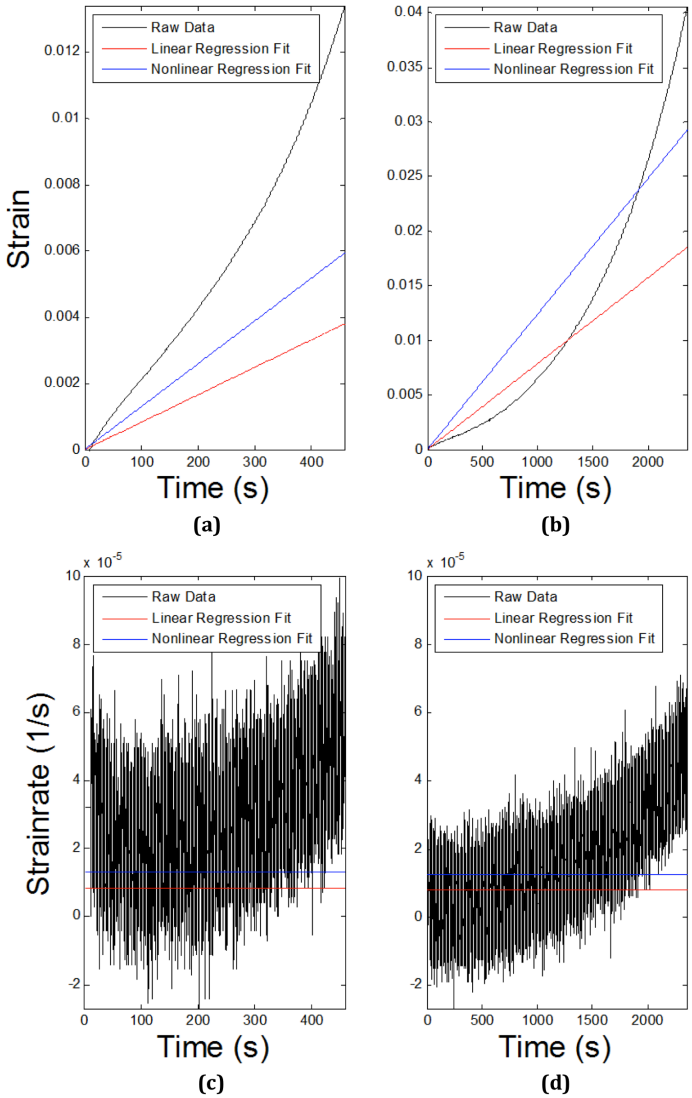

Figure 4-25: Exponential law model fitted to 6061 Al creep curves

For the 6061, the exponential model does a better job predicting the secondary region. With high stress curves, both sets of coefficients come closer to matching the secondary region. On the low stress end there is a little discrepancy. The coefficients from the linear regression do a better job as a predictor, but as with the nonlinear regression coefficients, still fail to predict the secondary region.

Upon conclusion of the exponential model a couple observations stand out. The power law does an overall better job as a predictor for creep curves. This observation is not based off any numbers, but a visual comparison of Figure 4-21, Figure 4-22, Figure 4-24 and Figure 4-25. Within just the exponential model, high stress is better matched than lower stress as expected by the nature of the exponential in the model. Still, by trying to model high and low stress, this model still fails to meet that standard.

4.4.4 Hyperbolic-Sine Creep Model

The final model examined for secondary creep predictions is a hyperbolic-sine model. This model, proposed by Garofalo, is a good alternative to the power law and exponential model **[22]**. While the other two models tend to work best for a certain range of stresses, a hyperbolic-sine model encompasses the entire range of stress.

$$\dot{\varepsilon} = Csinh(\alpha\sigma)^m exp\left(\frac{-Q}{RT}\right) \qquad \text{Equation 4-7}$$

Unknowns include C (s^{-1}), α (MPa^{-1}), and m (unitless) with the other variables the same as defined in the previous creep models. The feature that makes this model the best choice is the hyperbolic-sine term. At small stresses the hyperbolic-sine term behaves as a small angle approximation and the hyperbolic-sine can be removed and the result is Equation 4-2, the power law model. When stress is larger, the nature of the hyperbolic-sine produces an exponential effect thus yielding Equation 4-5, the exponential model.

Once again the unknown variables were determined using the linear and nonlinear regression methods. The linearized equation for the hyperbolic-sine is shown here.

$$ln\big(sinh(\alpha\sigma)\big) = \frac{ln\left(\dot{\varepsilon}exp\left(\frac{Q}{RT}\right)\right) - ln(C)}{m} \qquad \text{Equation 4-8}$$

Before doing anything with the equation, one major issue has to be addressed. There is an unknown variable in the dependent term of the equation. This makes it impossible to use the equation unless some other known value is substituted for alpha. A very rough estimate for alpha would be to substitute beta and n from the exponential and power law models.

$$\alpha = \frac{\beta}{n} \qquad \text{Equation 4-9}$$

By using this substitution Equation 4-8 can be solved for the rest of the unknowns. This is completed with Figure 4-26.

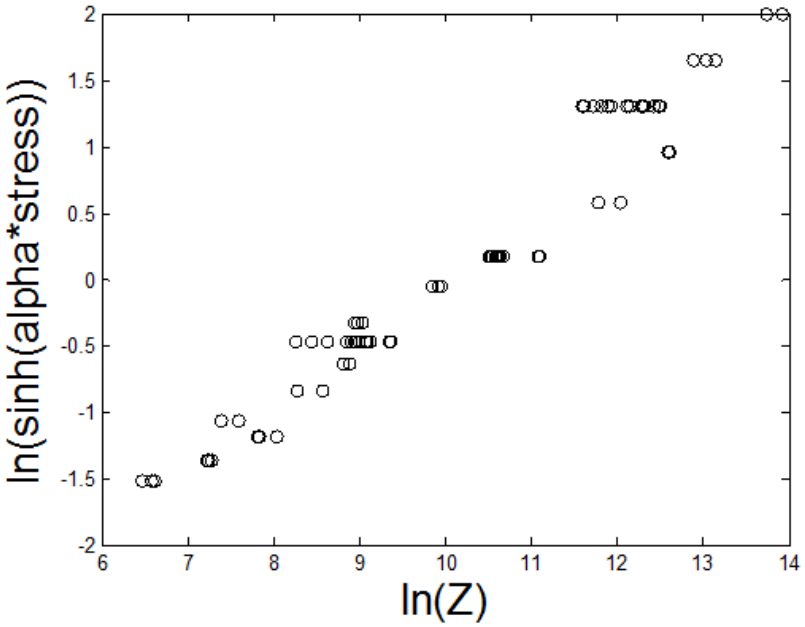

Figure 4-26: Data for hyperbolic-sine creep model fitting for 5083 Al

Comparing Figure 4-26 to Figure 4-20 and Figure 4-23 already shows the benefits of this model. In the previous two models there was a nonlinear portion that caused the poor fitting results. This plot only shows linearity already indicating a better chance of fitting the creep data. Moving on to the analysis, the linear and nonlinear regressions were completed and summarized in Table 4-5.

Table 4-5: Hyperbolic-sine creep model unknowns

	C (s^{-1})	α (MPa^{-1})	m	C (s^{-1})	α (MPa^{-1})	m
Linear Regression	2.03×10^{4}	0.017	2.00	5.63×10^{5}	0.012	2.66
Nonlinear Regression	1.24×10^{5}	0.010	2.42	8.45×10^{4}	0.031	1.33

Applying these values to Equation 4-7 will show how accurately it can predict high and low stress creep curves. For 5083 the curves examined are a 200°C 160MPa, Figure 4-27a,c, and a 400°C 13MPa creep curve, Figure 4-27b,d.

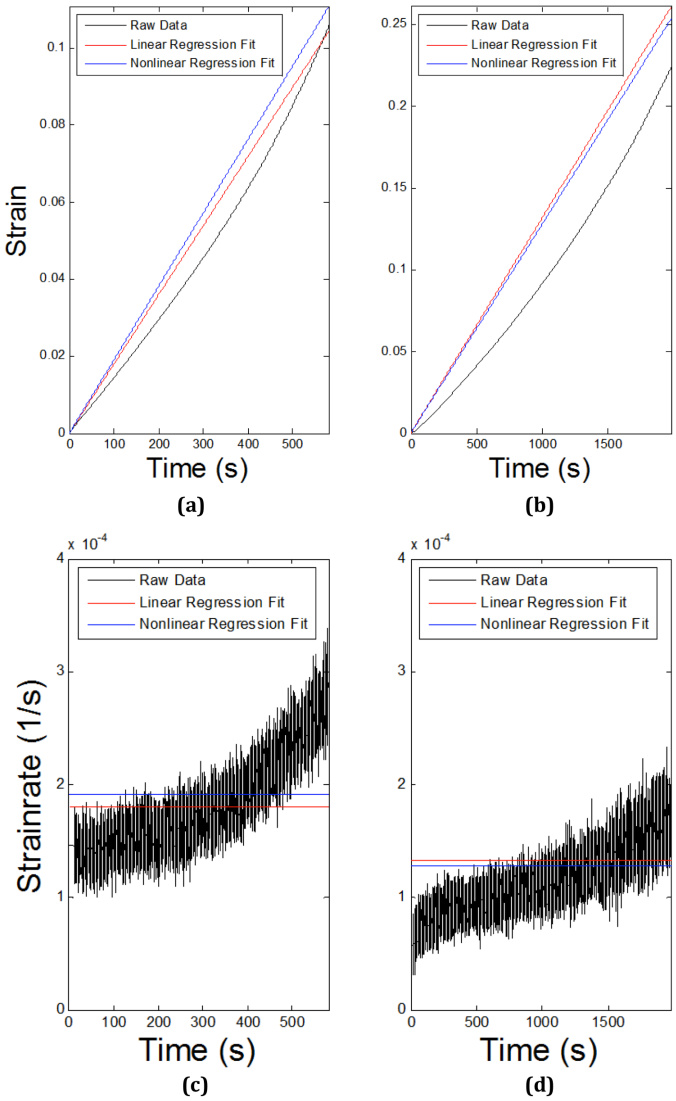

Figure 4-27: Hyperbolic-sine creep model fitted to 5083 Al creep curves

The hyperbolic-sine model still does not completely fit the secondary region, but is an overall improvement over the previous two models based on visual inspection. While the other models could only come close to measuring either high or low stress, the hyperbolic-sine improves on both. Even though the model is not quite ideal, it is an improvement in the right direction. The 6061 creep data shows a similar result.

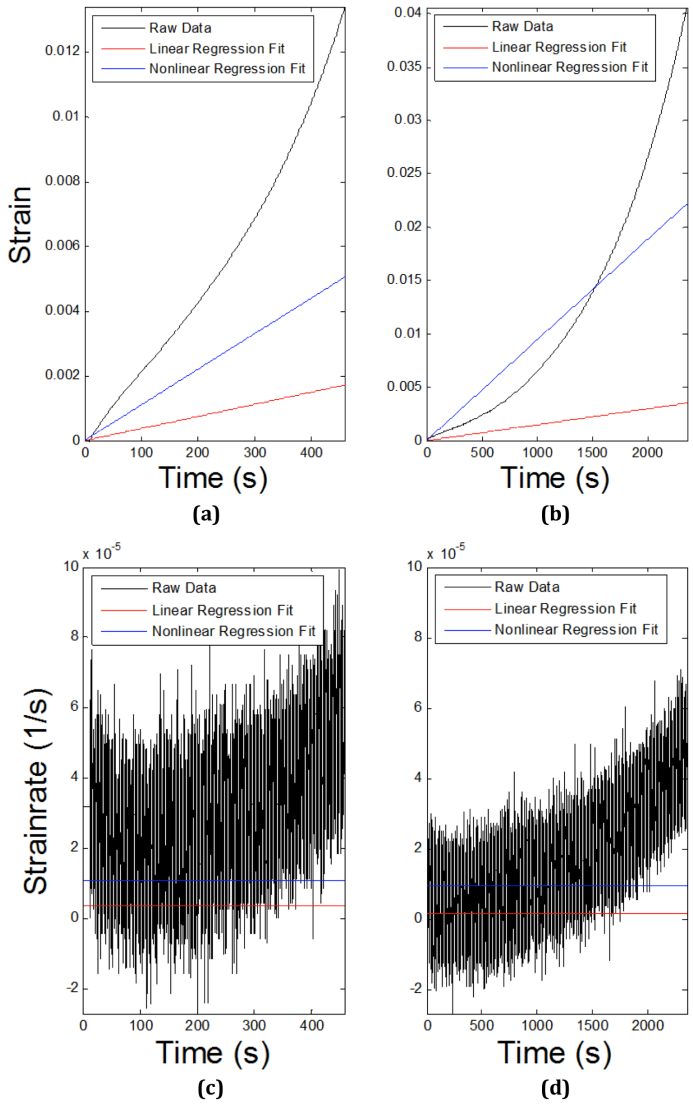

Figure 4-28: Hyperbolic-sine creep model fitted to 6061 Al creep curves

For 6061, the hyperbolic-sine model does a much better job fitting the high and low stress creep curves. These curves represent a 200°C 220MPa, Figure 4-28a,c, and a 400°C 13MPa, Figure 4-28b,d, creep test. While it is still not a perfect match to the secondary region, it is still an improvement indicating the potential for a creep model that can accurately model high and low stress creep curves.

While still not able to predict high and low stress creep curves, the hyperbolic-sine model has the most potential. The power law and exponential law models did better jobs in their respective regimes, low or high stress, but the hyperbolic-sine came closer to modeling the entire range of creep data.

CHAPTER 5 – Summary and Conclusions

With the completion of this work, it is now time to look over everything that was done and draw conclusions based on the results and analysis. The first step completed was elevated temperature tensile testing. For these tests, the 5083 and 6061 samples were heated to temperatures that ranged from room temperature to 500°C in increments of 50°C. Multiple tests were run at each temperature using two different extensometers, a mechanical and laser. After the tests were completed strength properties, including elastic modulus, yield strength, and ultimate strength, were measured reported for each temperature. The reduction of area was also calculated for each material as a measure of ductility.

Upon conclusion of the tensile testing, creep testing was done over a range of 200 to 400°C and stresses between 13 and 220MPa for 6061, and 13 and 160MPa for 5083. From the creep tests, the steady-state strain rate was measured from the secondary region and used as the basis for examining the effects of stress and temperature on the materials. From there, three creep models were examined as a means of predicting the secondary creep region.

5.1 Conclusions for Elevated Temperature Tensile Testing

Before drawing any conclusions about the tensile tests, it would be beneficial to look back at the goals of the tests that were defined in Chapter 1.3. The goal was to characterize the strength of the material under elevated temperature conditions. That goal was completed with the testing and showed a couple interesting trends. In both materials the elastic modulus was measured from the elastic region of the test. Results from these measurements should a fairly linear decline in stiffness as the temperature increased. While this may seem logical, the real story is how much the modulus value changes. 5083 changes from a stiffness of 71 to 15GPa and 6061 changes from 67 to 12GPa. At 500°C, the 15GPa and 12GPa elastic modulus values mean that the material is very soft. This soft corresponds to a small elastic region meaning the potential for a permanent strain to occur in the material is very likely.

Yield strength and ultimate strength were also measured as part of the strength characterization of the materials. These two properties had the same behavior with strength remaining relatively constant and high up to 150°C before plummeting to almost nothing at 400°C. From 400 to 500°C, the strengths steadily declined to an almost zero strength value. These materials showed quite a change in strength over the testing range. For 5083 the yield strength changed from 276MPa at room temperature to 15MPa at 500°C, while the ultimate strength dropped from 346MPa at room temperature to 17MPa at 500°C. 6061 dropped from 319 to 9MPa and 332 to 11MPa for yield strength and ultimate strength respectively. These are very dramatic changes in strength that show a substantial weakening of the material especially over the range of 200 to 300°C.

The final measurement completed was the reduction of area measurements. These measurements showed the trend of increasing ductility with the increasing

temperature. While that fact is not surprising, the interesting results occur after the temperature reaches 400°C. After this point the ductility decreases corresponding to a change in failure modes that exhibits more of a brittle behavior as opposed to a ductile failure.

The important thing now is to relate these results to a real application, i.e. a fire on a naval ship. From the results of the tensile testing, a high temperature fire would be detrimental to a naval ship that utilizes these aluminums. At low temperatures, up to 150°C, the material would be weakened, but not to a point where failure is a strong possibility. However, if the fire get hotter, the strength starts to degrade at a much faster pace making failure of any structural pieces much more likely.

5.2 Conclusions for Creep Testing

The goal of the creep testing was to develop an understanding of the effects of temperature and stress on the materials over extended periods of time. To measure these effects, creep tests were completed at temperatures ranging from 200 to 400°C with a variety of stresses between 13 and 220MPa. In order to determine how temperature and stress affect the materials, a stress was applied to a heated sample and strain was measured until failure. After failure, the steady-state strain rate was determined from the secondary region of the creep curve. This provided a means of comparing the temperature and stress, strain rate, and the full creep curve. The full creep curves provided a good visualization of the data and made it very clear what was happening with temperature and stress. The results of these test showed that temperature and stress play a very critical role in creep behavior. Even though no two temperatures had the same stress measurements, using the tests completed provided a good idea of what would happen. Using 6061 as an example a creep test completed at 200°C and 200MPa took approximately 1hr 30min. Using the highest stress tested at 250°C, 150MPa, at 200°C the creep test would likely go for at least half a day. If it was reversed and 200MPa was tested at 250°C, the sample would most likely fail during loading or just after the stress is reached.

The other aspect measured was strain rate. This will provide an indication for how fast the sample is creeping under a particular stress and temperature. Strain rate measurements can also relate back to the fire scenario. If a fire is occurring at a certain temperature for an extended period of time, it is mimicking a creep test. Knowing the loads caused by structural members and other equipment on top of an aluminum structure in a fire, the strain rate could tell how quickly strain will increase in the material and a creep model could then predict the behavior and failure.

5.3 Conclusions for Creep Modeling.

Creep modeling was the final aspect of this work. The goal was to find a model that would be suitable for predicting the secondary creep behavior over the whole range of temperatures and stresses that were completed with the creep testing. Three models were examined as a means of predicting creep behavior, a power law creep model,

exponential model, and hyperbolic-sine model. Each of these models had there own strengths and weaknesses making each one slightly better for different situations.

The power law model was better suited for low stress applications. Upon finding the two unknown parameters the model was used to predict the secondary creep region of a high and low stress creep test. Low stress was decently predicted using this model, but high stress was not. Improvements to the model can be made fitting to just low stresses.

Next was the exponential model. Unlike the power law model, the exponential model was better at predicting high stress. Using the same methods as the power law model, the unknown constants were determined and plotted against low and high stress creep curves. Better predictions were made on the high stress curve, and can be improved by fitting model parameters to only high stress data points.

A hyperbolic-sine model was the last model examined. High and low stress were better predicted using this model. At low stresses, the model could be reduced to the power law, and at high stresses, the behavior of the hyperbolic-sine is exponential like. The one disadvantage of this model is there are three unknown parameters to determine meaning the only way to determine these values is through a nonlinear analysis or by using an inexact substitution for one of the unknowns. Regardless of the difficulties, the unknowns were determined and plotted against the same high and low stress creep curves of the previous two models. While the model did not completely predict the secondary creep region, it was an overall improvement over the entire range.

To conclude the creep modeling, the best approach seems to be using a combination of the first two models, power law and exponential, to model high and low stress creep tests, or refine the hyperbolic-sine model to use the one equation. As mentioned in the goals of modeling, an important aspect of the creep model is incorporation with a finite element program, specifically Abaqus. Abaqus has built in capabilities to handle a power law and hyperbolic-sine models. This indicates that the hyperbolic-sine model would be a better choice for modeling than the combination of power law and exponential models.

CHAPTER 6 – Recommendations for Future Work

A lot of information regarding the high temperature response of 5083 and 6061 aluminum was covered in this work. A characterization of strength properties was completed from room temperature to 500°C and creep testing were done over a variety of strengths and temperatures. Modeling work was also completed on the creep data to try and predict the secondary region using three different models. While all this information and analysis is helpful, it can be expanded on to make the analysis even better and more comprehensive.

6.1 Future Work for Elevated Temperature Tensile Testing

Elevated temperature tensile testing is a pretty straightforward part of this work. Tensile tests were performed over a wide range of temperatures and strength properties determined for all these tests. Potential for future work in this area lies in two areas. First is the continuation of strength characterization to temperatures near the melting point of the aluminum, approximately 590°C. It would be beneficial to know how much strength changes between 500°C and melting temperature. Does the strength slowly decay to zero, or does it remain constant to a point then abruptly disappear?

A second interest in elevated temperature tensile testing would be to examine the strain rate sensitivity of the materials at elevated temperatures. Work has been done to examine the strain rate sensitivity of the materials at room temperature and has shown some interesting behavior, especially with the 5083 **[34]**. At room temperature, 5083 has a negative strain rate sensitivity. It would be interesting to know if this behavior occurs at 500°C or what temperature this behavior disappears, if it all.

6.2 Future Work for Creep Testing

Testing already completed for creep covered a wide range of temperature and stress. To expand on this testing, lower and/or higher temperatures can be explored as well as expanding the stress range at each temperature. However, the testing completed already covers a wide range that further testing may not provide any extra benefits. More effort on creep modeling would be much more beneficial than more creep testing.

6.3 Future Work for Creep Modeling

Creep modeling has the most potential for future expansion. What was seen from the creep modeling was attempts to predict the secondary creep region using a power law, exponential, and hyperbolic-sine creep model. As said they are only used as predictors for secondary creep. Expansion can be completed by attempting to model creep in the primary and tertiary regions of the creep curve. A model for primary and tertiary creep modeling was already suggested by Maljaars, but may not be the best model for the stress

and temperatures tested in this work **[24]**. Other models for tertiary creep include a damage evolution model proposed by Kachanov and Rabotnov **[35, 36]** This model would require a measure of reduction of area as the sample necks and fails.

In order to attempt these models, equipment other than that used in this work would have to be utilized. None of the equipment, mechanical or laser extensomter, have the capabilities to measure the damage evolution of the sample. To complete this, a digital image correlation (DIC) system would most likely have to be used which could present more/different issues with high temperature application.

References

[1] Sielski, R. A. (1987). "THE HISTORY OF ALUMINUM AS A DECKHOUSE MATERIAL." Naval Engineers Journal 99(3): 165-172.

[2] Voorhees, H. R. and J. W. Freeman (1960). Report on the elevated-temperature properties of aluminum and magnesium alloys. Philadelphia, American Society for Testing Materials.

[3] Volkl, R. and B. Fischer (2004). "Mechanical testing of ultra-high temperature alloys." Proceedings of the Society for Experimental Mechanics, Inc 51: 121-127.

[4] Codrington, J., P. Nguyen, et al. (2009). "Induction heating apparatus for high temperature testing of thermo-mechanical properties." Applied Thermal Engineering 29(14-15): 2783-2789.

[5] Taleff, E. M., G. A. Henshall, et al. (1998). "Warm-temperature tensile ductility in Al-Mg alloys." Metallurgical and Materials Transactions A: Physical Metallurgy and Materials Science 29A(3 A): 1081-1091.

[6] Harun, H. J. and P. G. McCormick (1979). "Effect of precipitation hardening on strain rate sensitivity and yield behaviour in an Al-Mg-Si alloy." Acta Metallurgica 27(1): 155-159.

[7] Huskins, E., B. Cao, et al. (2012). "Temperature-Dependent Mechanical Response of an UFG Aluminum Alloy at High Rates." Experimental Mechanics 52(2): 185-194.

[8] Van Liempt, P. and J. Sietsma (2011). "A revised criterion for the portevin-Le chatelier effect based on the strain-rate sensitivity of the work-hardening rate." Metallurgical and Materials Transactions A: Physical Metallurgy and Materials Science 42(13): 4008-4014.

[9] Taleff, E. M., P. J. Nevland, et al. (2001). "Tensile ductility of several commercial aluminum alloys at elevated temperatures." Metallurgical and Materials Transactions A (Physical Metallurgy and Materials Science) 32A(5): 1119-1130.

[10] Ozturk, F., S. Toros, et al. (2008). "Evaluation of tensile properties of 5052 type aluminum-magnesium alloy at warm temperatures." Archives of Materials Science and Engineering 34(2): 95 - 98.

[11] Khalifa, T. A. and T. S. Mahmoud (2009). Elevated Temperature Mechanical Properties of Al Alloy AA6063/SiCp MMCs. World Congress on Engineering, WCE 2009, 1-3 July 2009, Hong Kong, China, International Association of Engineers.

[12] Amdahl, J., N. Kristin Langhelle, et al. (2001). Aluminium plated structures at elevated temperatures. 20th International Conference on Offshore Mechanics and Arctic Engineering; Safety and Reliability, June 3, 2001 - June 8, 2001, Rio de Janeiro, Brazil, American Society of Mechanical Engineers.

[13] Das, S., A. R. Riahi, et al. (2012). "High temperature deformation and fracture of tribo-layers on the surface of AA5083 sheet aluminum-magnesium alloy." Materials Science and Engineering A 531: 76-83.

[14] Clausen, A. H., T. Brvik, et al. (2004). "Flow and fracture characteristics of aluminium alloy AA5083-H116 as function of strain rate, temperature and triaxiality." Materials Science and Engineering A 364(1-2): 260-272.

[15] Leitao, C., R. Louro, et al. (2012). "Analysis of high temperature plastic behaviour and its relation with weldability in friction stir welding for aluminium alloys AA5083-H111 and AA6082-T6." Materials & Design 37: 402-409.

[16] Kaibyshev, R., F. Musin, et al. (2005). "Deformation behavior of a modified 5083 aluminum alloy." Materials Science and Engineering a-Structural Materials Properties Microstructure and Processing 392(1-2): 373-379.

[17] Yavari, P., F. A. Mohamed, et al. (1981). "Creep and substructure formation in an Al-5% Mg solid solution alloy." Acta Metallurgica 29(8): 1495-1507.

[18] Park, K. T., E. J. Lavernia, et al. (1994). "HIGH-TEMPERATURE DEFORMATION OF 6061-AL." Acta Metallurgica Et Materialia 42(3): 667-678.

[19] Harper, J. G. and J. E. Dorn (1956). Viscous Creep of Aluminum Near Its Melting Temperature. United States: 34p.

[20] Feltham, P. and J. D. Meakin (1961). "On the activation energy of high temperature creep." Acta Metallurgica 9(11): 1036-1037.

[21] Dorn, J. E. (1955). "Some fundamental experiments on high temperature creep." Journal of the Mechanics and Physics of Solids 3(2): 85-116.

[22] Garofalo, F., 1965, Fundamentals of Creep and Creep-Rupture in Metals, Macmillan, New York

[23] Harmathy, T. Z. (1967). "A comprehensive creep model." Transactions of the ASME. Series D, Journal of Basic Engineering 89(3): 496-502.

[24] Maljaars, J. (2008). Local Buckling of Slender Aluminium Sections Exposed to Fire, Technische Universiteit Eindhoven.

[25] Penny, R. K. and D. L. Marriott (1971). Design For Creep. London, McGraw-Hill.

[26] "Accessories Catalog for Materials Testing." *Instron : Including Grips, Fixtures, Extensometers, Load Cells, Furnaces and More to Enhance Your Test System*. N.p., n.d. Web. 19 Nov. 2012.

[27] Benedyk, J. C. (2009). "International Temper Designation Systems for Wrought Aluminum Alloys: *Part I - Strain Hardenable (H Temper) Aluminum Alloys* " Light Metal Age: 26-30.

[28] "ASM Material Data Sheet." Aluminum 5083-H116; 5083-H321. Retrieved November 3, 2012, from http://asm.matweb.com/search/SpecificMaterial.asp?bassnum=MA5083H116.

[29] Benedyk, J. C. (2010). "International Temper Designation Systems for Wrought Aluminum Alloys: *Part II - Thermally Treated (T Temper) Aluminum Alloys*." Light Metal Age: 16-22.

[30] "ASM Material Data Sheet." Aluminum 6061-T6; 6061-T651. Retrieved November 3, 2012, from http://asm.matweb.com/search/SpecificMaterial.asp?bassnum=MA6061t6.

[31] Saha, G. G., P. G. McCormick, et al. (1984). "Portevin-Le Chatelier effect in an Al-Mn alloy. I. Serration characteristics." Material Science and Engineering 62(2): 187-196.

[32] Saha, G. G., P. G. McCormick, et al. (1984). "Portevin-Le Chatelier effect in an Al-Mn alloy. II. Yield transition and strain rate sensitivity measurements." Material Science and Engineering 62(2): 197-203.

[33] *Eurocode 9: Design of Aluminium Structures*. London: BSI, 1999. Print.

[34] Romhanji, E., A. Dudukovska, et al. (2002). "The effect of temperature on strain-rate sensitivity in high strength Al-Mg alloy sheet." Journal of Materials Processing Technology 125: 193-198.

[35] Kachanov, L. M., 1967, The Theory of Creep, National Lending Library for Science and Technology, Boston Spa, England, Chaps. IX, X.

[36] Rabotnov, Y. N., 1969, Creep Problems in Structural Members, North Holland, Amsterdam.

Appendix A – Tensile Testing

Chapter 3 discussed the elevated temperature tensile tests and showed graphical representations of the results. As a reference this section shows the numerical results used in the formation of those charts.

Table A-1: Elevated temperature tensile testing results for 5083 Al

Temperature (°C)	Elastic Modulus (GPa)	Yield Strength (MPa)	Ultimate Strength (MPa)	Reduction of Area (%)
25 (Room Temp)	70	275	344	18.15
25 (Room Temp)	71	276	343	17.04
25 (Room Temp)	70	277	348	17.32
25 (Room Temp)	74	276	347	14.72
50	71	279	346	12.72
50	69	279	347	15.06
50	71	276	343	14.81
50	72	278	344	13.08
100	66	271	328	16.80
100	67	272	332	15.65
100	67	275	334	15.12
100	67	271	335	14.77
150	62	247	281	40.18
150	62	253	284	40.54
150	61	251	286	38.73
150	62	249	283	39.83
200	54	219	228	71.36
200	55	215	227	71.09
200	50	219	230	71.46
200	54	213	227	69.34
250	44	137	156	87.50
250	43	142	158	87.66
250	42	148	161	87.36
250	44	133	159	85.64
300	41	88	89	97.05
300	43	88	91	96.49
300	41	89	90	96.85
300	44	89	90	95.91
350	37	68	70	97.57
350	36	67	70	97.65
350	37	67	69	97.49
350	36	70	70	97.44
400	26	44	48	94.83
400	27	44	48	95.44
400	28	44	47	95.58
400	28	48	49	95.80
450	18	24	28	90.43
450	19	24	31	92.65
450	22	26	31	88.72
450	20	29	30	90.64
500	16	16	18	77.90
500	16	15	18	84.97
500	15	15	18	69.58
500	14	15	15	74.29

This first table shows the results from all the tensile tests for 5083. The next set of data comes from the tensile testing for 6061.

Table A-2: Elevated temperature tensile testing results for 6061 Al

Temperature (°C)	Elastic Modulus (GPa)	Yield Strength (MPa)	Ultimate Strength (MPa)	Reduction of Area (%)
25 (Room Temp)	66	317	330	30.76
25 (Room Temp)	63	319	331	30.59
25 (Room Temp)	69	319	332	31.18
25 (Room Temp)	70	322	336	36.54
50	73	311	323	39.74
50	74	310	321	39.85
50	66	314	326	39.72
50	67	316	329	39.85
100	69	296	301	42.90
100	65	298	304	44.03
100	70	299	304	48.68
100	66	301	307	48.57
150	62	277	277	54.90
150	66	280	280	55.32
150	66	281	281	55.47
150	62	282	282	57.60
200	64	239	239	61.87
200	59	234	234	61.27
200	57	241	241	61.08
200	59	253	253	65.05
250	56	177	177	48.08
250	56	174	175	46.81
250	53	180	181	47.15
250	52	177	178	43.93
300	43	101	103	66.09
300	44	104	106	67.20
300	50	103	106	67.24
300	46	96	100	73.33
350	41	62	64	79.98
350	42	61	65	80.18
350	40	64	67	80.96
350	41	67	71	80.58
400	29	32	34	93.76
400	33	31	33	94.07
400	29	28	30	93.97
400	33	34	37	93.94
450	20	12	14	97.90
450	20	12	14	97.57
450	21	13	15	97.40
450	19	15	17	99.61
500	11	8	10	95.18
500	13	8	10	95.03
500	14	9	11	96.84
500	10	10	12	97.24

Appendix B – Creep Testing Numerical Values

While Chapter 4 showed the results of the creep testing, there were not any numerical values for a reference. To remedy this, the numerical results are shown here. First are the results from the 5083 creep test.

Table B-1: Strain rate for 5083 Al creep testing

Temperature (°C)	Stress (MPa)	Strain Rate Excel (s^{-1})	Strain Rate Matlab (s^{-1})
200	160	1.83E-04	1.83E-04
200	160	1.52E-04	1.52E-04
200	160	1.52E-04	1.52E-04
200	140	6.52E-05	6.52E-05
200	140	7.59E-05	7.59E-05
200	140	8.48E-05	8.48E-05
200	120	3.57E-05	3.57E-05
200	120	4.33E-05	4.33E-05
200	120	4.13E-05	4.13E-05
250	100	4.29E-04	4.29E-04
250	100	4.18E-04	4.18E-04
250	80	2.39E-04	2.38E-04
250	80	1.86E-04	1.86E-04
250	60	9.23E-05	9.23E-05
250	60	9.35E-05	9.37E-05
300	50	1.57E-04	1.59E-04
300	50	1.78E-04	1.85E-04
300	50	1.69E-04	1.69E-04
300	40	6.46E-05	6.46E-05
300	40	7.04E-05	7.13E-05
300	40	6.65E-05	6.65E-05
300	35	3.23E-05	3.26E-05
300	35	4.72E-05	4.72E-05
300	35	3.88E-05	3.88E-05
350	30	2.73E-04	2.72E-04
350	30	2.50E-04	2.52E-04
350	25	1.46E-04	1.50E-04
350	25	1.97E-04	1.98E-04
350	20	6.12E-05	6.12E-05
350	20	7.46E-05	7.47E-05
400	18	4.15E-04	4.20E-04
400	18	3.38E-04	3.38E-04
400	18	3.33E-04	3.35E-04
400	15	1.82E-04	1.82E-04
400	15	1.86E-04	1.86E-04
400	15	1.93E-04	1.93E-04
400	13	1.01E-04	1.00E-04
400	13	8.67E-05	8.70E-05
400	13	9.56E-05	9.56E-05

Following the results from the creep tests are the 5083 results from the activation energy tests.

Table B-2: Strain rate for 5083 Al activation energy tests

Temperature (°C)	Stress (MPa)	Strain Rate Excel (s^{-1})	Strain Rate Matlab (s^{-1})
150	120	1.57E-06	1.50E-06
160	120	2.24E-06	2.24E-06
170	120	4.01E-06	4.02E-06
180	120	9.27E-06	9.26E-06
190	120	1.91E-05	1.91E-05
200	120	3.63E-05	3.62E-05
150	120	2.12E-06	2.05E-06
160	120	2.53E-06	2.50E-06
170	120	5.28E-06	5.29E-06
180	120	1.10E-05	1.10E-05
190	120	2.26E-05	2.25E-05
200	120	4.42E-05	4.41E-05
200	60	7.10E-06	7.34E-06
210	60	1.07E-05	1.07E-05
220	60	1.68E-05	1.70E-05
230	60	2.62E-05	2.65E-05
240	60	3.83E-05	3.87E-05
250	60	5.87E-05	5.90E-05
200	60	6.53E-06	6.68E-06
210	60	9.73E-06	9.82E-06
220	60	1.55E-05	1.56E-05
230	60	2.40E-05	2.43E-05
240	60	3.48E-05	3.52E-05
250	60	5.21E-05	5.25E-05
250	30	1.67E-05	1.73E-05
260	35	1.90E-05	1.94E-05
270	35	2.45E-05	2.48E-05
280	35	3.00E-05	3.01E-05
290	35	4.47E-05	4.51E-05
300	35	6.84E-05	6.87E-05
250	35	1.62E-05	1.69E-05
260	35	1.86E-05	1.91E-05
270	35	2.30E-05	2.32E-05
280	35	3.16E-05	3.18E-05
290	35	4.68E-05	4.71E-05
300	35	7.24E-05	7.26E-05

The next set of data comes from the full creep tests performed on the 6061 aluminum.

Table B-3: Strain rate for 6061 Al creep testing

Temperature (°C)	Stress (MPa)	Strain Rate Excel (s^{-1})	Strain Rate Matlab (s^{-1})
200	220	1.34E-05	1.34E-05
200	220	2.18E-05	2.16E-05
200	220	1.39E-05	1.39E-05
200	210	4.83E-06	4.82E-06
200	210	5.72E-06	5.71E-06
200	210	3.37E-06	3.35E-06
200	200	1.90E-06	1.90E-06
200	200	1.54E-06	1.53E-06
200	200	1.83E-06	1.84E-06
250	150	8.74E-06	8.75E-06
250	150	1.44E-05	1.46E-05
250	140	3.19E-06	3.21E-06
250	140	5.20E-06	5.19E-06
250	130	1.53E-06	1.54E-06
250	130	1.98E-06	1.97E-06
300	80	3.68E-06	8.39E-06
300	80	7.22E-06	7.29E-06
300	80	7.25E-06	7.36E-06
300	70	2.89E-06	2.92E-06
300	70	3.35E-06	3.33E-06
300	70	3.68E-06	3.68E-06
300	60	1.47E-06	1.46E-06
300	60	1.75E-06	1.76E-06
300	60	1.42E-06	1.42E-06
350	50	1.85E-05	1.84E-05
350	50	2.93E-05	2.90E-05
350	45	7.32E-06	7.24E-06
350	45	9.02E-06	8.94E-06
350	40	3.63E-06	3.61E-06
350	40	5.29E-06	5.29E-06
400	20	3.14E-05	3.10E-05
400	20	1.93E-05	1.94E-05
400	20	2.56E-05	2.57E-05
400	15	8.10E-06	8.04E-06
400	15	6.08E-06	6.00E-06
400	15	5.70E-06	5.72E-06
400	13	5.43E-06	5.48E-06
400	13	5.11E-06	4.90E-06
400	13	5.39E-06	5.40E-06

The final set of data for creep testing comes from the activation energy tests complete for 6061.

Table B-4: Strain rate for 6061 Al activation energy tests

Temperature (°C)	Stress (MPa)	Strain Rate Excel (s^{-1})	Strain Rate Matlab (s^{-1})
200	130	1.62E-07	9.16E-07
210	130	1.51E-07	2.37E-07
220	130	2.23E-07	2.20E-07
230	130	6.01E-07	6.08E-07
240	130	1.49E-06	1.44E-06
250	130	2.38E-06	2.32E-06
200	130	1.79E-07	2.23E-07
210	130	2.49E-07	2.47E-07
220	130	2.85E-07	1.52E-07
230	130	5.74E-07	5.67E-07
240	130	7.24E-07	7.61E-07
250	130	1.62E-06	1.63E-06
250	70	2.40E-07	3.43E-07
260	70	2.31E-07	1.87E-07
270	70	5.35E-07	5.62E-07
280	70	5.94E-07	5.92E-07
290	70	1.14E-06	1.22E-06
300	70	2.92E-06	2.93E-06
250	70	2.65E-07	6.56E-07
260	70	2.50E-07	2.60E-07
270	70	5.14E-07	4.75E-07
280	70	4.66E-07	5.02E-07
290	70	1.43E-06	1.42E-06
300	70	3.08E-06	3.07E-06